1964

Gamma-ray penetration of iron-lead shields

Vishvanath Dattatraya Chitnis
Iowa State University

GAMMA-RAY PENETRATION OF IRON-LEAD SHIELDS

by

Vishvanath Dattatraya Chitnis

A Dissertation Submitted to the
Graduate Faculty in Partial Fulfillment of
The Requirements for the Degree of
DOCTOR OF PHILOSOPHY

Major Subject: Nuclear Engineering

Approved:

Signature was redacted for privacy.
In Charge of Major Work

Signature was redacted for privacy.
Head of Major Department

Signature was redacted for privacy.
Dean of Graduate College

Iowa State University
Of Science and Technology
Ames, Iowa

1964

TABLE OF CONTENTS

INTRODUCTION

The problem of gamma ray shielding is closely associated with the problem of reactor shielding. It arises from the fact that gamma rays are emitted along with neutrons in a neutron chain reactor.

In the design of shields for either nuclear reactors or pure gamma radiation sources it is often felt that the thickness of the shields used is overestimated. The conservative estimate results from the calculations based on approximate formulas.

In the case of mobile reactors or radiation sources it is desirable to reduce the weight of the shield as much as possible. Also it is necessary to absorb most of the radiation in the shield so that the level of the dose rate at the outer edge of the shield is below the maximum permissible level.

Thus, the problem of designing a shield for a radiation source is basically important for two reasons. Firstly, it is necessary to study the transport of radiation across the thickness of the shield as accurately as possible. The transport of radiation depends upon the cross sections of the materials used for the construction of the shields. The cross section which is mainly responsible for the transport of radiation is the scattering cross section. Secondly, the problem requires a new approach in the design of the shield itself. Thus far

the shields used consist of one or two materials. The slabs of the materials are kept side by side.

In the problem under study in this investigation a laminated shield is designed for a source of gamma radiation. The shield consists of alternate alyers of iron and lead. The innermost layer is made up of iron. The conventional two region shield is replaced by a multi-region shield.

REVIEW OF LITERATURE

The problem of the penetration of gamma radiation through thick layers of material was considered for the first time by Hirschfelder *et al*. (1, 2). Klein-Nishina scattering is applied to a wide homogeneous monochromatic beam of gamma rays striking a slab of material at right angles. The range of energy for which the method is applicable is small. The approach is used for gamma rays emitted by many naturally occurring and some artificial radioactive substances. The problem is treated exactly for both the unscattered and the once scattered fluxes. It is assumed that most of the scattered radiation makes only a small angle with the forward direction, and the multiple scattered radiation does not make any significant contribution to the total intensity. As long as the average angle of scattering is small, this gives good results. But in general this is not the case.

A similar approach was used by Bethe *et al*. (3). They treated the problem by considering the progressive simultaneous processes of energy degradation, multiple scattering and absorption. At high energies Compton scattering involves very small angles. Therefore, a photon penetrates through a thick slab of material almost in a straight line. This works very well as long as the energy of the photon is high. When the energy is degraded to a value where it undergoes large angle

scattering, the method is not useful. The same approach was elaborated further by Fano (4).

Peebles and Plesset (5) have used a similar approach only for heavy elements. Photons which have undergone few scatterings are considered for transmission. The probability that a photon is transmitted after n collisions is calculated by using Klein-Nishina differential cross section. The energy of the photon is computed by using this probability. The numerical integration of the probability function becomes difficult when the number of collisions is large.

The straight ahead solution obtained by Bethe et al. (3) was modified further by Solon and Wilkins (6) in order to consider the effect of scattering at various angles. An effective cross section was defined which takes into account scattering at various angles and the average of the reciprocal of the angle of scattering taken over the angular distribution of the scattered photons. It turned out to be a slight improvement over the straight ahead method (7). It is good in the case of heavy elements. An excellent review of the above mentioned approaches is given by Fano et al. (8).

There have been many attempts to solve the transport equation for photons. Since the cross sections and especially the Klein-Nishina differential scattering cross section are very complicated functions of energy and the scattering angle, thus far, rigorous solutions have not been obtained. Even the

numerical solution of the transport equation is extremely laborious.

The Monte Carlo method or the method of random sampling has proven valuable in the case of numerical solution. The trajectory of a photon is followed completely by locating its position in space and the result of each successive elementary interaction experienced by the photon up to its subsequent absorption is studied. It is not possible to predict these events exactly. Because of the random nature of quantum phenomena, only their probability distribution can be predicted. The Monte Carlo method is an analog of a real physical process. The imitation of the physical process is carried through by using random numbers.

Goldstein (9) gives a brief introduction to the applicability of the Monte Carlo method to shielding problems. Kahn (10, 11, 12) has discussed some problems in which this method is used. The general nature of this problem is discussed by Meyer (13).

The method is well suited for the solution of problems in shielding. It is extremely flexible and can be applied to problems involving complex boundary conditions. On the other hand, laborious calculation is an inherent and weak feature of the method.

Zerby (14) used the Monte Carlo approach to calculate penetration of gamma rays through slabs of plastic and lead.

Beach *et al.* (15) have used the technique to estimate gamma ray spectral intensities for shallow and deep penetration. The transport of gamma rays through thick slabs of lead was also studied by Kalos (16).

OBJECTIVE

The objective of the investigation was to develop a procedure, based on the Monte Carlo techniques, for the determination of the energy absorption rate of gamma rays in a laminated shield.

In order to determine the dose rate along the thickness of the shield, due to a source of gamma radiation, it is necessary to study the energy distribution of gamma rays in the entire thickness of the shield and obtain the energy deposited as gamma rays penetrate through the shield.

The shield is infinite in two dimensions and finite in one dimension. The finite dimension is taken along the x-axis. The shield consists of alternate layers of iron and lead of constant thickness. The maximum number of layers is determined from the total thickness of the shield. The total thickness was calculated in the case of a point isotropic source of gamma rays emitting photons of energy $10moc^2$, to reduce the dose rate at the outer edge of the shield to maximum permissible level. This thickness was estimated to be 18 cm in the case of shield consisting of iron only.

Thus, the total thickness of the shield was kept constant throughout the investigation. The ratio of the thickness of iron slab to that of the adjacent lead slab is defined as γ. This ratio is varied and the transport of gamma rays is studied

across the finite dimension of the shield. Four different ratios of γ are used. These range between 0.5 and 5.0.

For each value of γ the energy absorbed per cm^3 per second along the x-axis in the shield is calculated. Thus, an analysis of laminated shields of iron and lead is made to obtain the dose rate across the total thickness of the composite shield.

The arrangement of the basic configuration of the composite shield is illustrated in Figure 1.

This calculation is based on a maximum permissible level of 2.5 mr/hr.

$$\frac{5.11 \text{ Mev}}{cm^3\text{-sec}} \cdot \frac{3600 \text{ sec/hr}}{67.7 \text{ Mev/}cm^3\text{-mr}} e^{-0.2436r} = 2.5 \frac{mr}{hr}$$

The distance r obtained from this expression is 18.88 cm.

Figure 1. Laminated shield of alternate iron and lead slabs

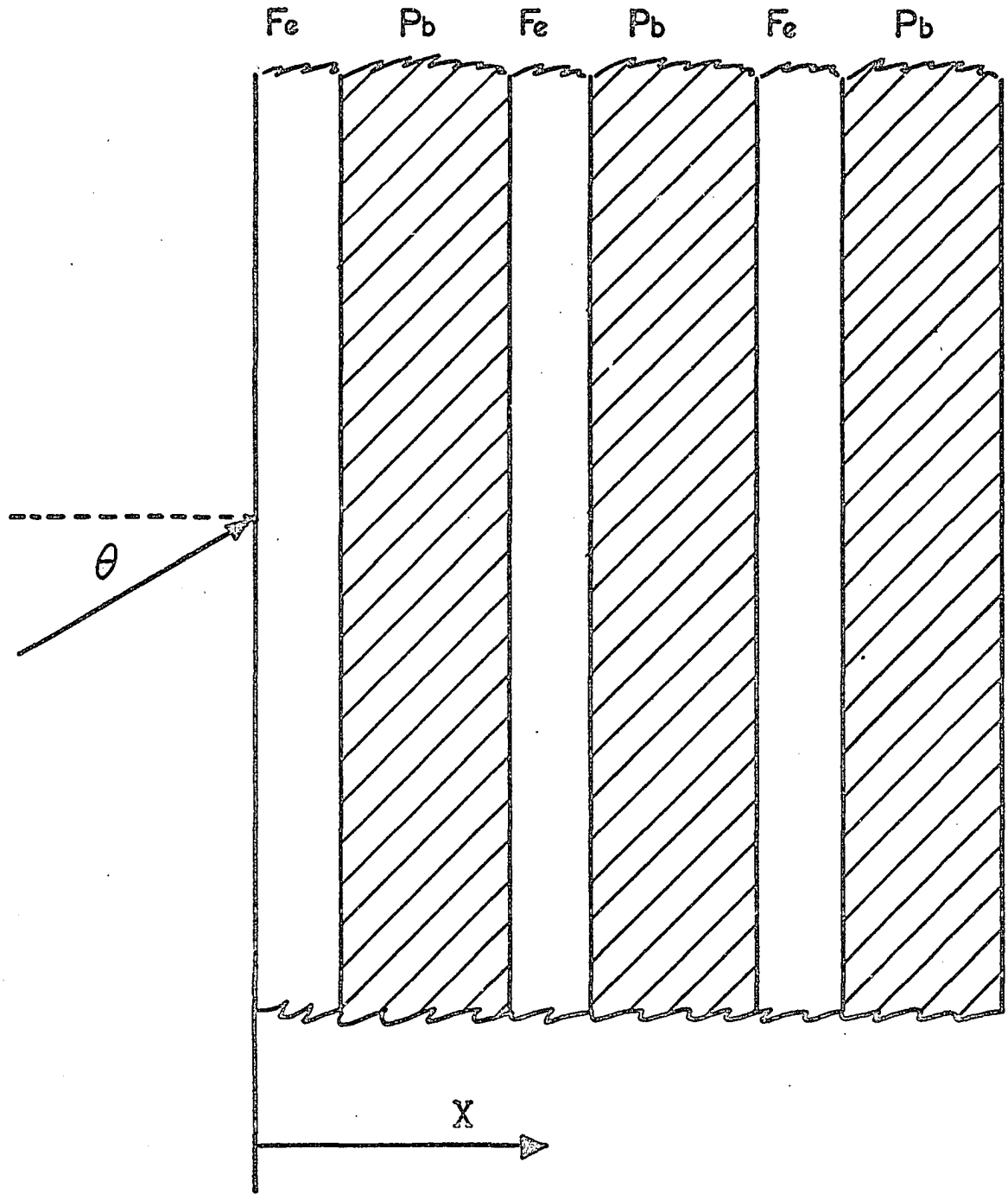
Fe
Pb
Fe
Pb
Fe
Pb
θ
X

INVESTIGATION

Procedure

The approach used in the problem under study is the Monte Carlo method or the method of random sampling. In this method a random number which is uniformally distributed over the interval 0 to 1 is chosen to determine the type of interaction a photon undergoes as it travels through the thickness of the shield.

Two different types of scatterings are used in this problem to study the transport of gamma rays in the shield. These are (i) Compton scattering and (ii) Elastic scattering.

In the case of Compton scattering type of interaction the energy of the scattered photon and the angle of scattering are determined from the Klein-Nishina differential cross section (17, 18). This is usually written in the following form:

$$\frac{d\sigma}{d\Omega}(E) = \left(\frac{1}{2} r_o^2\right) \frac{(1+\alpha^2)}{\left[1+E(1-\alpha)\right]^2} \left\{ 1 + \frac{E^2(1-\alpha)^2}{(1+\alpha^2)\left[1+E(1-\alpha)\right]} \right\} \quad (1)$$

where

α = cosine of the scattering angle

$r_o = \frac{e^2}{moc^2} = 0.28183 \times 10^{-12}$ cm

E = energy of incident photon in units of moc^2

The energy of the scattered photon is given by

$$E' = \frac{E}{1 + E(1-\alpha)} \tag{2}$$

The angle of scattering is obtained from equation 2. In terms of E and E' it can be written as

$$\alpha = 1 + \frac{1}{E} - \frac{1}{E'} \tag{3}$$

In order to determine the energy of the scattered photon and the angle of scattering random numbers are used.

Upon substituting equation 3 into equation 1 and changing the variable from Ω to E the differential cross section becomes

$$\frac{d\sigma}{dE} = \frac{\pi r_o^2}{E^2} \left\{ \left(\frac{1}{E'} - \frac{1}{E}\right)^2 - 2\left(\frac{1}{E'} - \frac{1}{E}\right) + \frac{E'}{E} + \frac{E}{E'} \right\} \tag{4}$$

A random number RAN is chosen to determine the energy of the scattered photon.

$$RAN = p(E' \leq E) \tag{5}$$

where

$p(E' \leq E)$ is the probability that the energy $E' \leq E$ and

$$p(E' \leq E) = \frac{\int_{E'}^{E} \frac{d\sigma}{dE'} \cdot dE'}{\sigma_{Compt}(E)} \tag{6}$$

where

$\sigma_{Compt}(E)$ is the microscopic Compton scattering cross section.

$$\sigma_{Compt}(E) = 2\pi r_o^2 \left[\frac{1+E}{(1+2E)^2} + \frac{2}{E^2} + \frac{(E^2-2E-2)}{2E^3} \ell n(1+2E) \right] \quad (7)$$

$$\int_{E'}^{E} \frac{d\sigma}{dE} \cdot dE = \frac{\pi r_o^2}{E^2} \left[2 + \frac{E}{2} + \frac{1}{E'} - \frac{E'}{E^2} - \frac{2E'}{E} - \frac{E'^2}{2E} \right] \quad (8)$$

Combining equations 5, 6, 7 and 8 the expression becomes

$$RAN \cdot \left[\frac{2E^2(1+E)}{(1+2E)^2} + 4 + \frac{(E^2-2E-2)}{E} \ell n(1+2E) \right] =$$

$$\left[2 + \frac{E}{2} + \frac{1}{E'} - \frac{E'}{E^2} - \frac{2E'}{E} - \frac{E'^2}{2E} - \frac{(E^2-2E-2)}{E} \ell n \frac{E'}{E} \right] \quad (9)$$

Expression 9 is solved analytically on the computer in order to determine E'. This value of E' is used in expression 3 to determine the cosine of the angle of scattering μ.

Now μ is the cosine of the angle between the path of the photon before and after the collision. The path of the photon after collision rotates through an azimuthal angle χ_i. χ_i is random on $(0, 2\pi)$. Thus the angle of scattering with respect to x-axis is given by the following relation (8):

$$\cos\theta_{i+1} = \cos\theta_i \mu + \sin\theta_i \sqrt{1-\mu^2} \cos\chi_i \quad (10)$$

The detailed flow diagrams for μ and E' are shown in Figures 8 and 9.

In the case of elastic type of scattering the energy of the incident photon is the same before and after the collision. The photon is scattered by the electron cloud in the

atom of the material. The angle of scattering is determined by using a random number.

Different routines are used for Fe and Pb. The energy dependence of the differential elastic cross section is determined from data given by Nelms and Opperheim (19).

In the case of Fe the best fit was obtained when the differential scattering cross section was written as the function

$$\frac{d\sigma}{d\Omega} = k_e^{-6.957\sqrt{1-c'}} \tag{11}$$

where

k = a numerical constant

c' = cosine of the angle between the path of the photon before and after scattering.

A random number G which is uniformly distributed over (0,1) is used to determine the scattering angle.

$$G = \frac{\int_{-1}^{C} \frac{d\sigma}{d\Omega} \cdot d\Omega}{\sigma_{elast}} \tag{12}$$

Equation 12 is solved analytically by using Newton-Raphson iteration method as mentioned in Hildebrand (20, p. 447). The detailed flow diagram is shown in Figures 11 and 12.

The elastic cross section for Pb is computed by Brenner et al. (21) and Brown and Mayers (22, 23). A fourth degree polynomial was fitted on the computer for the differential

scattering cross section of Pb. It has the form

$$\frac{d\sigma}{d\Omega} = A_5 + A_4 c' + A_3 c'^2 + A_2 c'^3 + A_1 c'^4 \qquad (13)$$

The values of A's are given in the flow diagram for Pb Elast Routine in Figure 13. A random number QAN is used to determine the angle of scattering using the expression:

$$QAN = \frac{\int_{-1}^{c} \frac{d\sigma}{d\Omega} \cdot d\Omega}{\sigma_{elast}} \qquad (14)$$

Equation 14 is solved analytically on the computer. The detailed flow diagram is shown in Figures 13 and 14.

In both cases the angle which the path of the scattered photon makes with the x-axis is determined from relation 10.

Main Program

The flow diagram describing the main program is given in Figure 2. The input parameters specified for the routine are the maximum energy EMAX, the minimum energy EMIN, total thickness of the shield, the number of layers in the shield, the thickness of each layer, and the number of histories to be generated in one run.

A point isotropic source emitting one photon per second is used in this investigation. The first collision is specified so that the angle between the slab normal and the direction of the emitted photon is between -90° and $+90^{\circ}$.

This ensures that each photon generates a history with at least one collision.

The photon enters the shield with energy 10 moc^2. The point at which it makes its first collision is determined by using a random number. The distance is determined according to exponential probability distribution (Appendix A). The macroscopic cross sections are determined from Subroutine Sigma. The flow diagrams for this subroutine are shown in Figures 2 and 3.

A random number is generated and compared with the ratio of Σ_{compt} to Σ_{total}. If the random number is less than or equal to this ratio, the interaction is considered to be Compton scattering. The program calls Subroutine Compt. If the number is less than or equal to the ratio of $(\Sigma_{compt} + \Sigma_{elast})$ to Σ_{total} and greater than the ratio of Σ_{compt} to Σ_{total}, then the interaction is considered to be elastic scattering. The program calls Subroutine Elast as indicated in Figure 3. In any other situation the interaction is considered to be an absorbing collision. Once the photon is absorbed the history is terminated and all the information regarding the absorbed photon is stored in the memory. This consists of the energy of photon at the time of absorption, the layer number, the distance in the layer, the number of Compton scatterings, and the number of elastic scatterings.

Sigma

In this subroutine macroscopic cross sections for Fe and Pb are computed. The selection of routine is made according to layer number as shown in Figure 4. If the layer number is odd the program follows the subroutine for Fe as shown in Figure 5. On the other hand if the number is even the program enters the subroutine for Pb shown in Figures 6 and 7. All the cross sections used in this work are taken from Grodstein (24).

The purpose of using this subroutine is not to block memory locations in the machine by way of stored input. Thus more memory locations are available for the output.

Compt

In this subroutine the energy of the scattered photon and its change in direction are computed. The difference in the energy before and after collision is considered to be absorbed and is deposited at the point of collision. The flow diagram for this subroutine is shown in Figures 8 and 9.

The Klein-Nishina distribution function is given by equation 1. By using a random number the relationship between the energy before and after collision is determined. This expression is solved analytically on the computer. All the steps involved in solving this expression are shown in detail in

Figures 8 and 9.

Once the energy after the Compton type of scattering is known the angle of scattering can be determined. This gives the angle with respect to the initial direction of the photon. The angle with respect to the slab normal is determined from equation 10.

Elast

The purpose of adding this subroutine to the program was to test the validity of using Rayleigh type of scattering along with Compton scattering. This type of scattering is practically negligible at high energies (3-10 Mev). Below 150 Kev energy it contributes about 6% to the total cross section. The flow diagrams are shown in Figures 10, 11, 12, 13, and 14.

Energy Absorption

The flow diagram shown in Figure 15 and Figure 16 illustrates the important steps of the Energy Absorption Subroutine. It forms a part of the Main Program. Since it is used to store output in a particular form, it is shown on a separate diagram.

In one history as the photon travels through the layers of the shield, it undergoes some number of Compton scattering collisions. In such a collision it loses a part of its energy. The part of the energy that is lost is considered

to be absorbed at the point of collision. It is deposited at the point of collision. The other process by which energy can be deposited is an absorbing collision.

The total thickness of the shield is 18 cm. An array of 18 columns is used in the computer and the magnitude of the energy is deposited in each column of the array depending upon the distance at which the energy is absorbed. In this way the total energy deposited in each run in each column is determined.

For each principal run 2400 histories were generated.

Figure 2. Main Routine

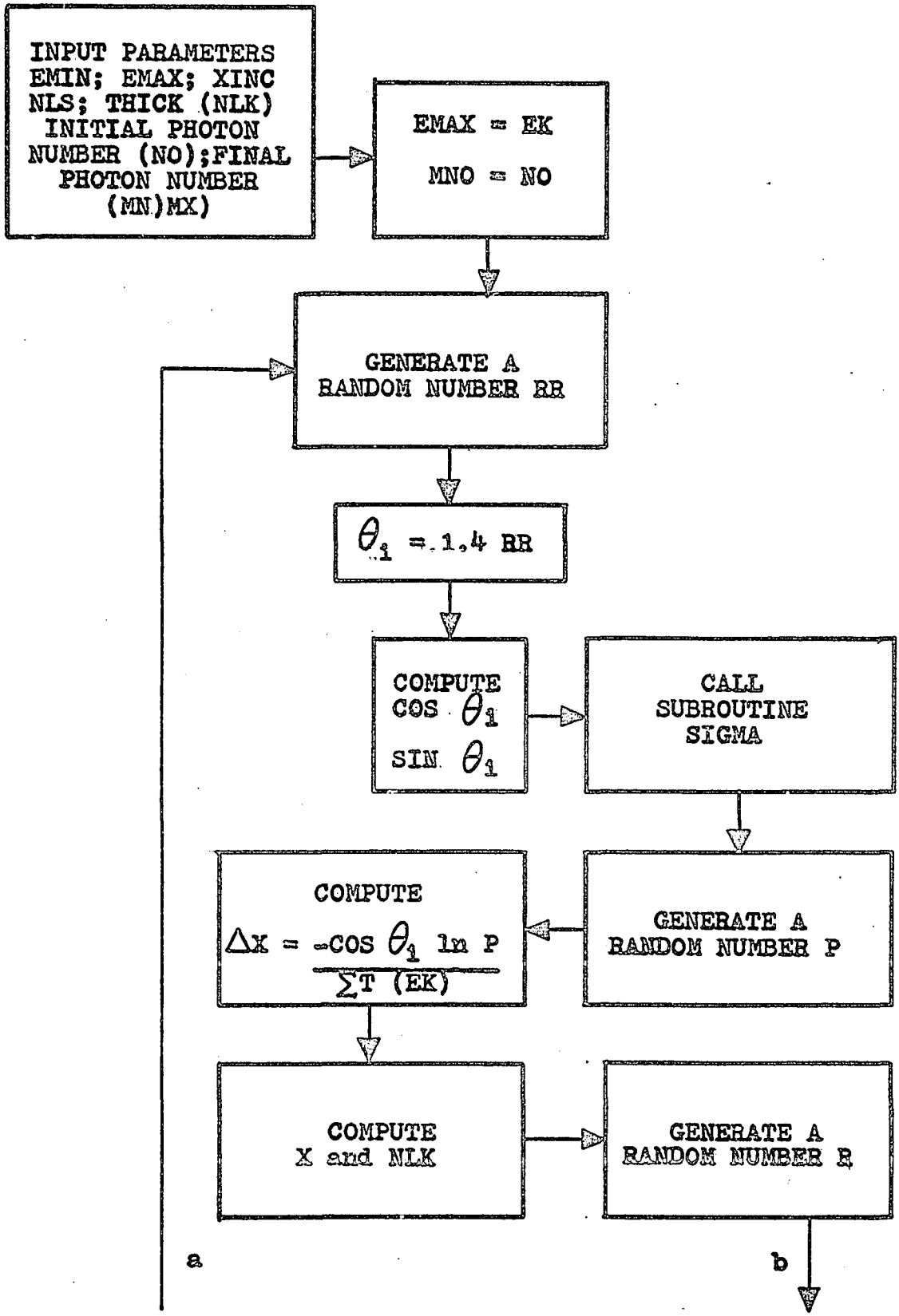
INPUT PARAMETERS EMIN; EMAX; XINC NLS; THICK (NLK) INITIAL PHOTON NUMBER (NO);FINAL PHOTON NUMBER (MN)MX)
EMAX = EK
MNO = NO
GENERATE A RANDOM NUMBER RR
θ_i = 1.4 RR
COMPUTE COS θ_i SIN θ_i
CALL SUBROUTINE SIGMA
GENERATE A RANDOM NUMBER P
COMPUTE $\Delta X = \frac{-\cos\theta_i \ln P}{\sum T (EK)}$
COMPUTE X and NLK
GENERATE A RANDOM NUMBER R
a
b

Figure 3. Completion of output from Main Routine

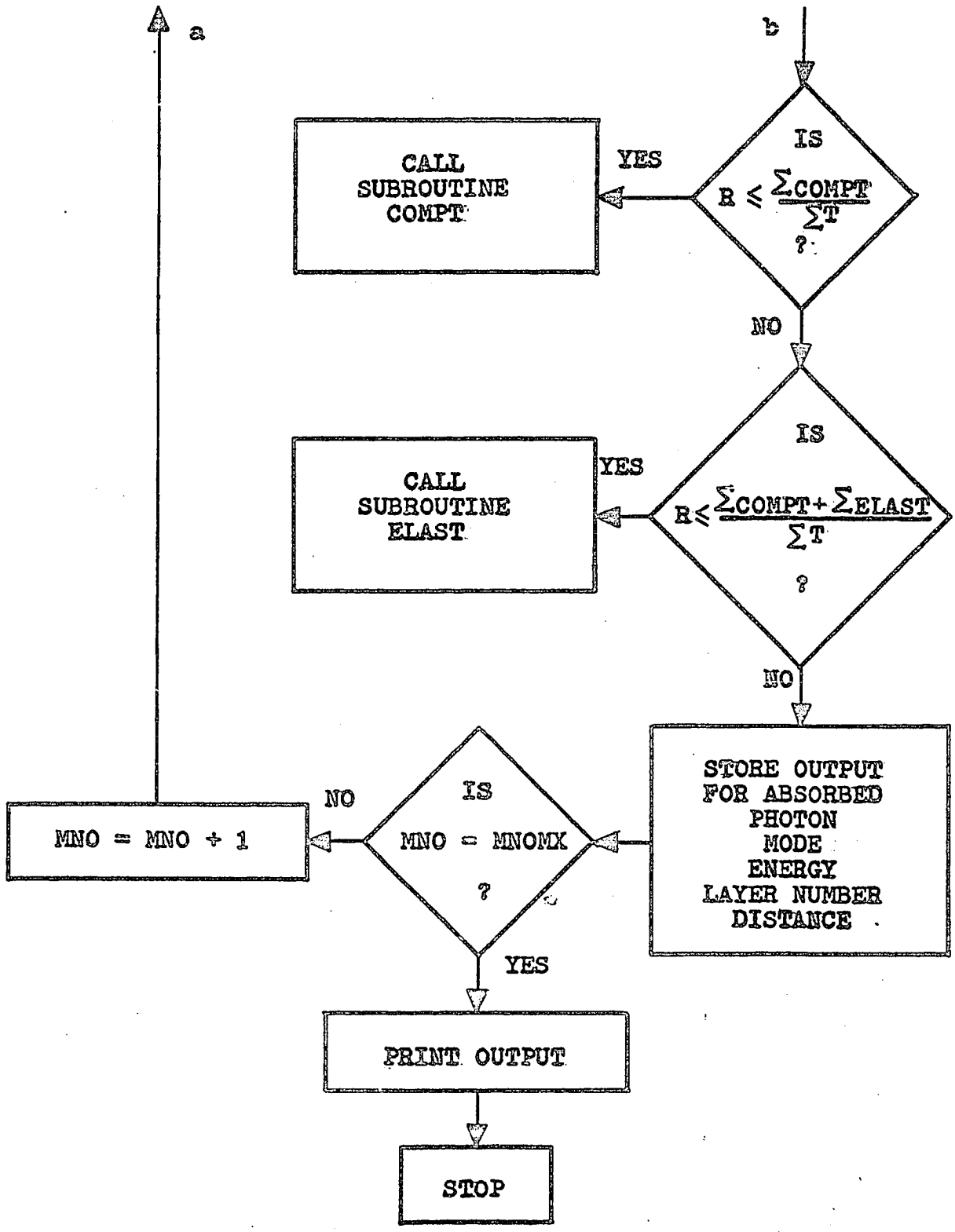
a
b
IS
R ≤ ΣCOMPT / ΣT
?
YES
CALL SUBROUTINE COMPT
NO
IS
R ≤ ΣCOMPT+ΣELAST / ΣT
?
YES
CALL SUBROUTINE ELAST
NO
STORE OUTPUT FOR ABSORBED PHOTON MODE ENERGY LAYER NUMBER DISTANCE
IS
MNO = MNOMX
?
NO
MNO = MNO + 1
YES
PRINT OUTPUT
STOP

Figure 4. Selection of layer to compute cross sections

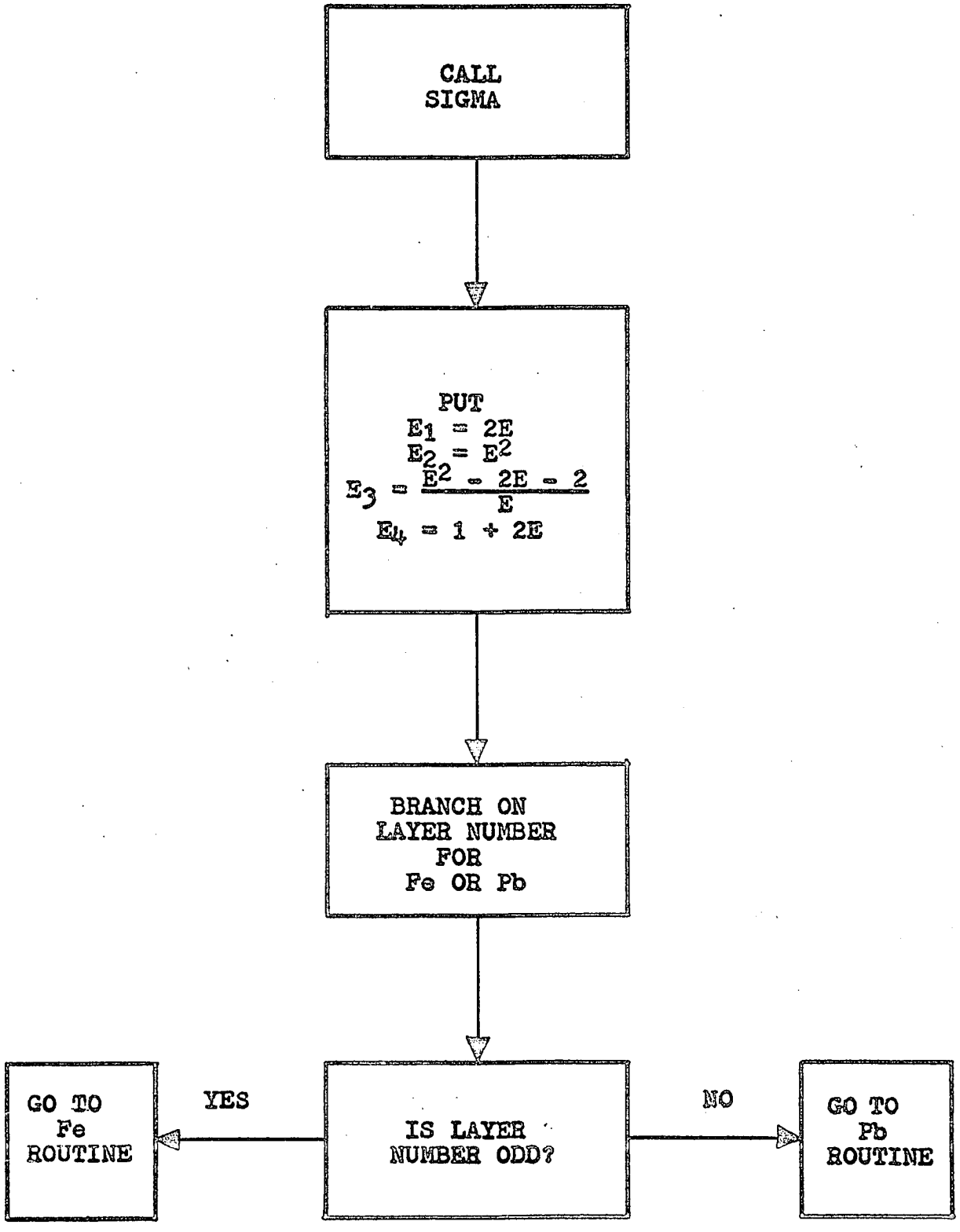
CALL
SIGMA
PUT
$E_1 = 2E$
$E_2 = E^2$
$E_3 = \frac{E^2 - 2E - 2}{E}$
$E_4 = 1 + 2E$
BRANCH ON
LAYER NUMBER
FOR
Fe OR Pb
IS LAYER
NUMBER ODD?
YES
NO
GO TO
Fe
ROUTINE
GO TO
Pb
ROUTINE

Figure 5. Cross sections routine for Fe

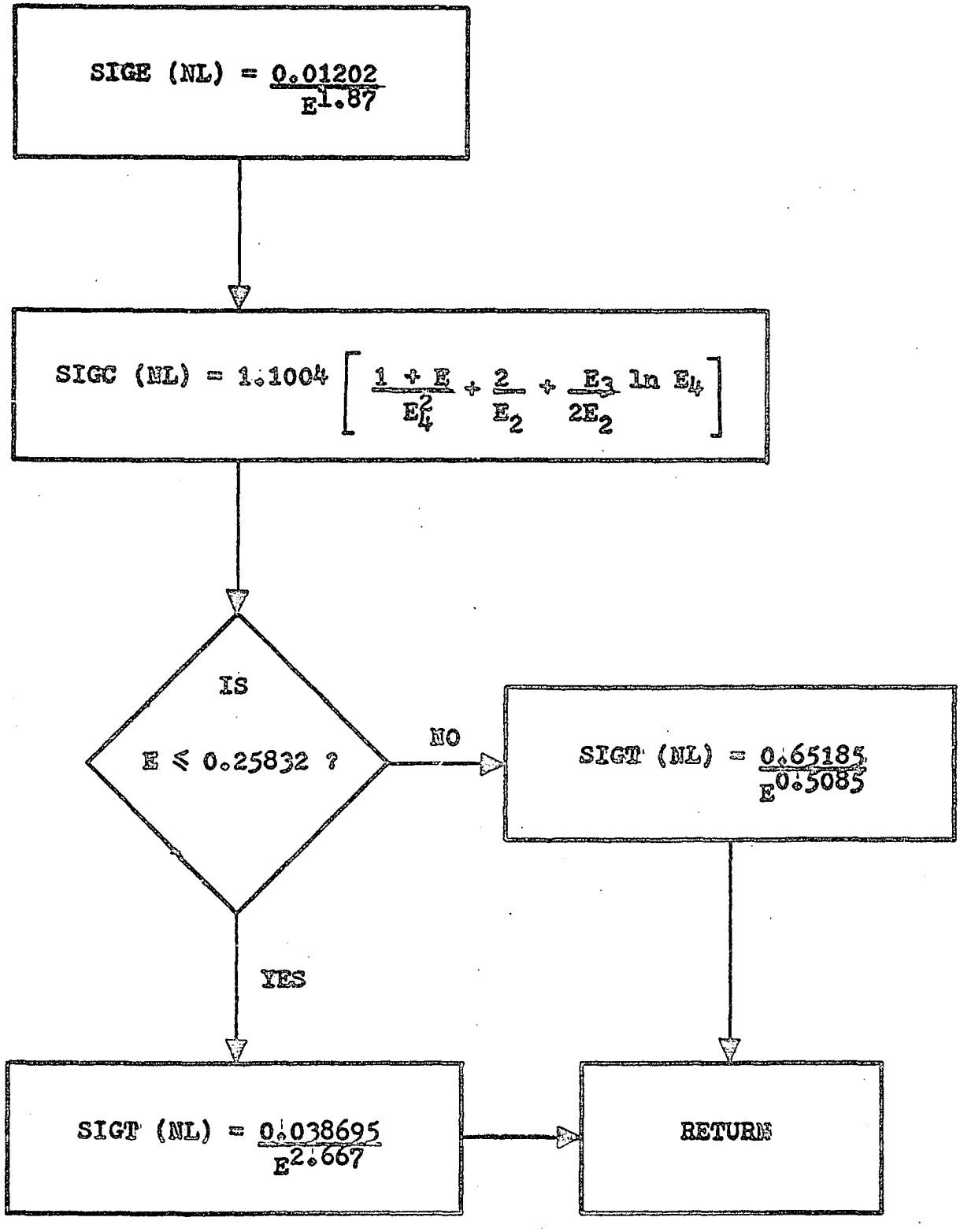
SIGE (NL) = 0.01202 / E^1.87
SIGC (NL) = 1.1004 [(1 + E)/E_4^2 + 2/E_2 + E_3/(2E_2) ln E_4]
IS
E ≤ 0.25832 ?
NO
SIGT (NL) = 0.65185 / E^0.5085
YES
SIGT (NL) = 0.038695 / E^2.667
RETURN

Figure 6. Start of cross sections routine for Pb

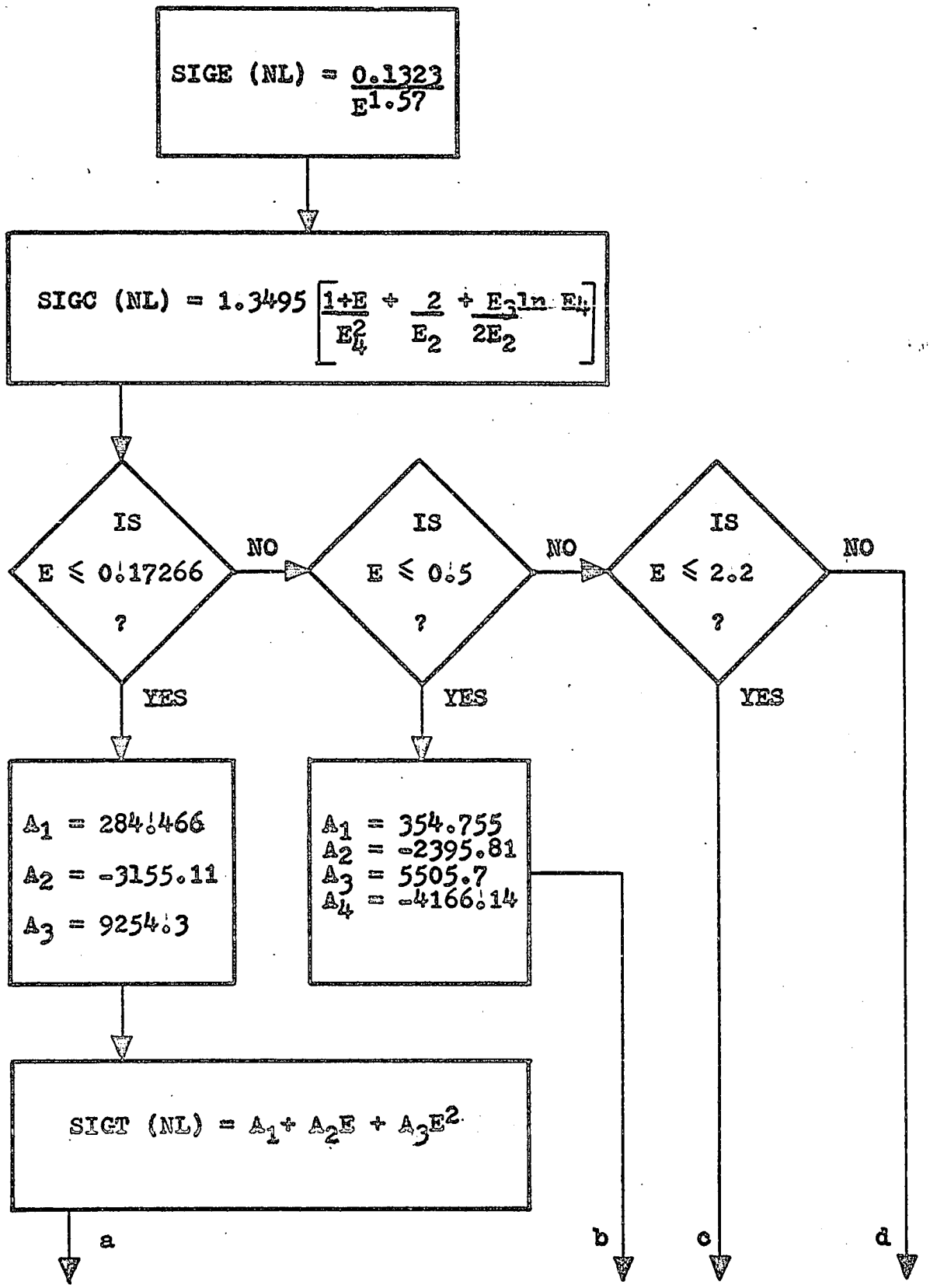
SIGE (NL) = 0.1323 / E^1.57
SIGC (NL) = 1.3495 [(1+E)/E4^2 + 2/E2 + E3 ln E4 / 2E2]
IS E ≤ 0.17266 ?
NO
IS E ≤ 0.5 ?
NO
IS E ≤ 2.2 ?
NO
YES
YES
YES
A1 = 284.466
A2 = -3155.11
A3 = 9254.3
A1 = 354.755
A2 = -2395.81
A3 = 5505.7
A4 = -4166.14
SIGT (NL) = A1 + A2E + A3E^2
a
b
c
d

Figure 7. Completion of cross sections routine for Pb

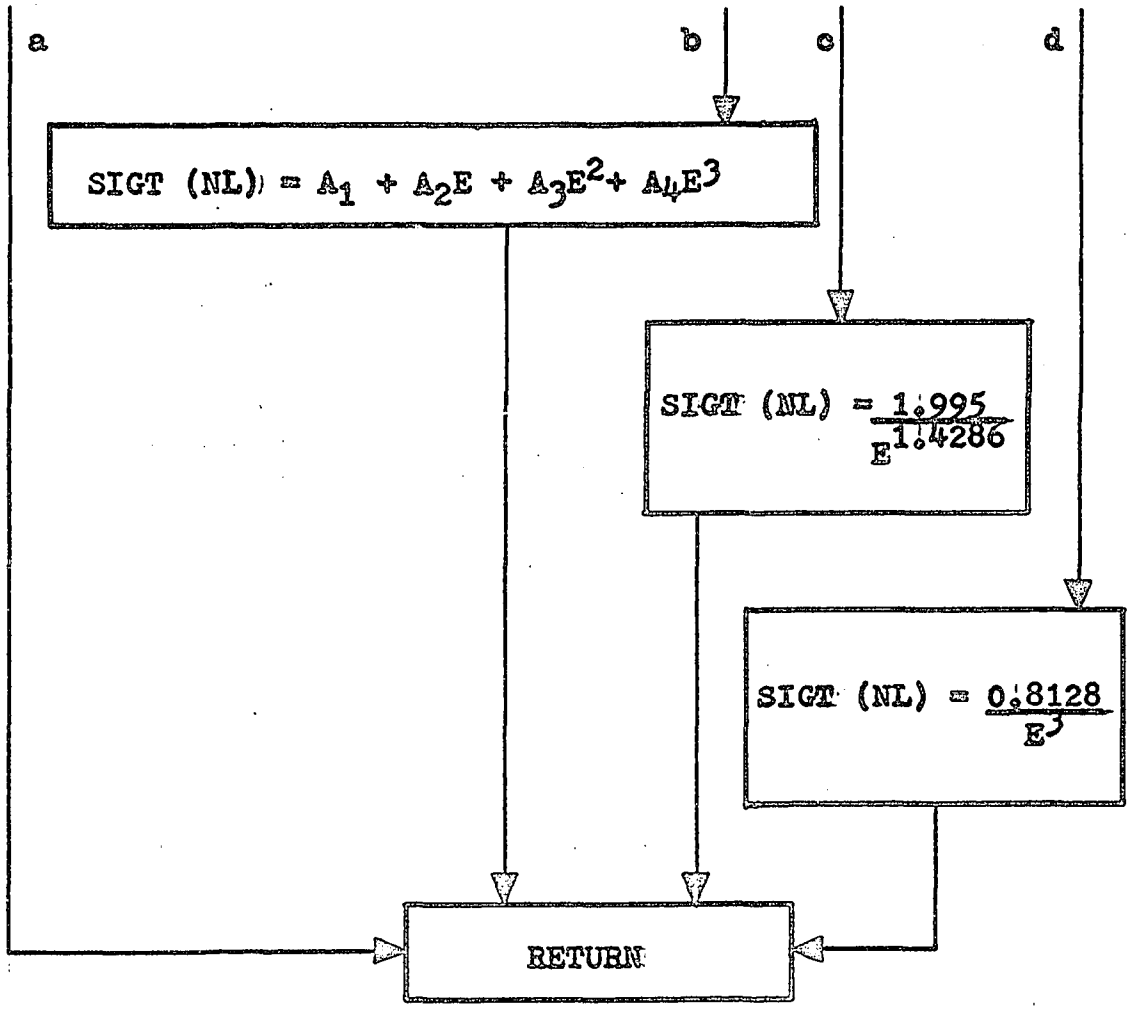
a
b
c
d
SIGT (NL) = $A_1 + A_2E + A_3E^2 + A_4E^3$
SIGT (NL) = $\frac{1.995}{E^{1.4286}}$
SIGT (NL) = $\frac{0.8128}{E^3}$
RETURN

Figure 8. Start of Compt subroutine with input parameters

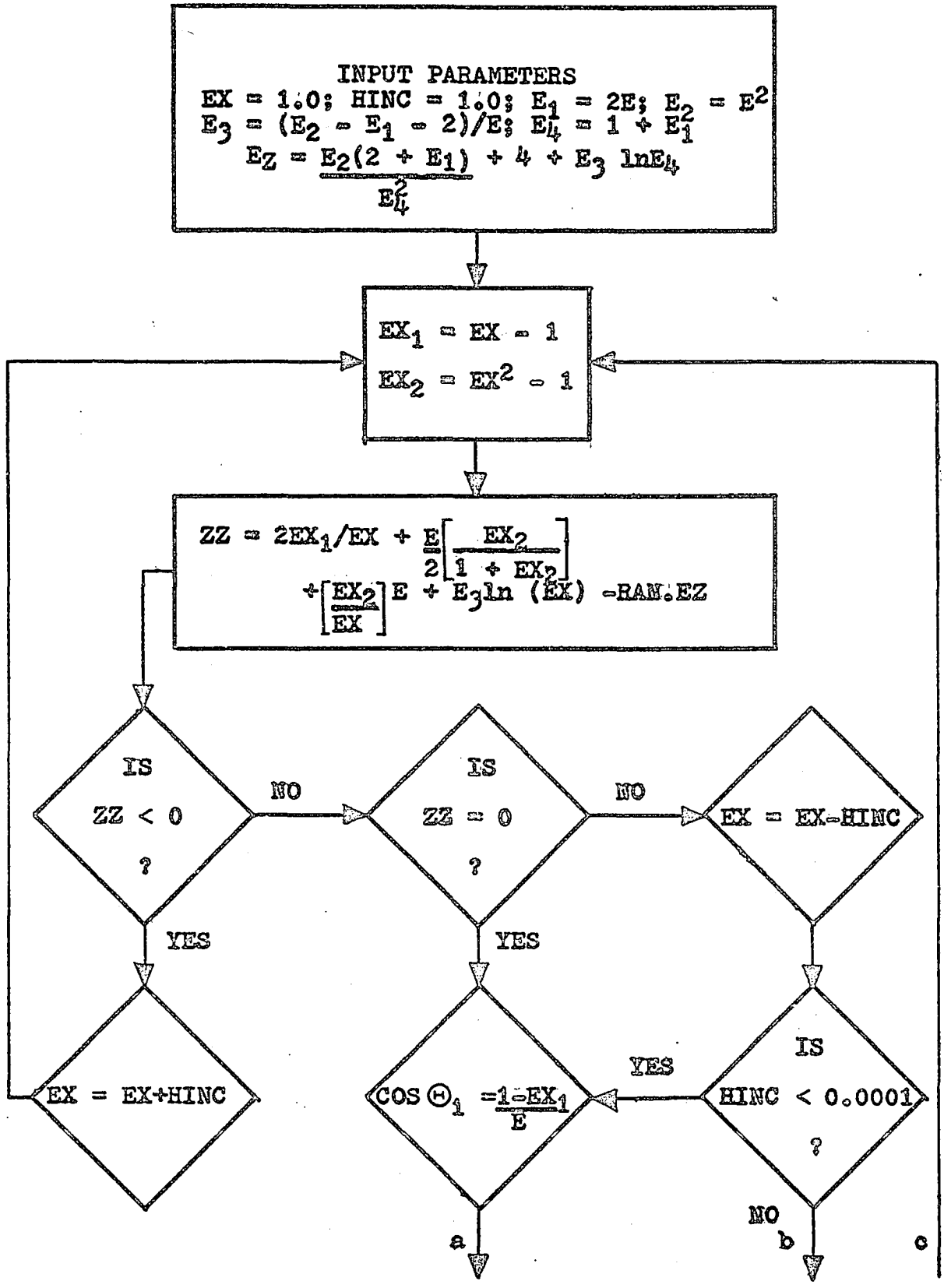
INPUT PARAMETERS
EX = 1.0; HINC = 1.0; $E_1 = 2E$; $E_2 = E^2$
$E_3 = (E_2 - E_1 - 2)/E$; $E_4 = 1 + E_1$
$E_Z = \frac{E_2(2 + E_1)}{E_4^2} + 4 + E_3 \ln E_4$
$EX_1 = EX - 1$
$EX_2 = EX^2 - 1$
$ZZ = 2EX_1/EX + \frac{E}{2}\left[\frac{EX_2}{1 + EX_2}\right] + \left[\frac{EX_2}{EX}\right] E + E_3 \ln(EX) - RAN.EZ$
IS ZZ < 0 ?
NO
IS ZZ = 0 ?
NO
EX = EX-HINC
YES
YES
EX = EX+HINC
$\cos\Theta_1 = \frac{1-EX_1}{E}$
YES
IS HINC < 0.0001 ?
NO
a
b
c

Figure 9. End of Compt subroutine with the change in energy and the angle of scattering

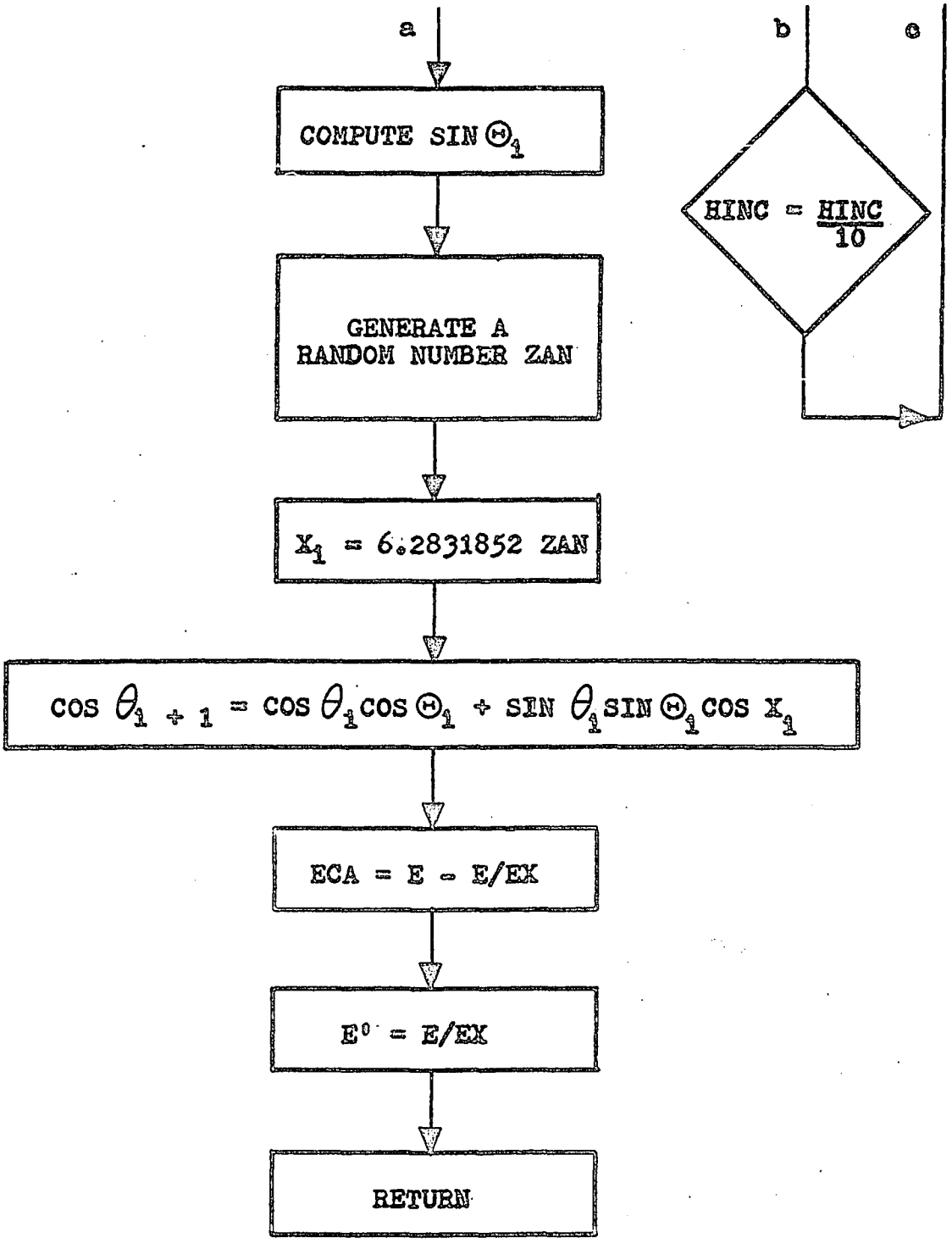
a
b
c
COMPUTE SIN Θ_1
HINC = HINC / 10
GENERATE A RANDOM NUMBER ZAN
X_1 = 6.2831852 ZAN
$\cos \theta_{1+1} = \cos \theta_1 \cos \Theta_1 + \sin \theta_1 \sin \Theta_1 \cos X_1$
ECA = E - E/EX
E^0 = E/EX
RETURN

Figure 10. Selection of layer for Elast subroutine

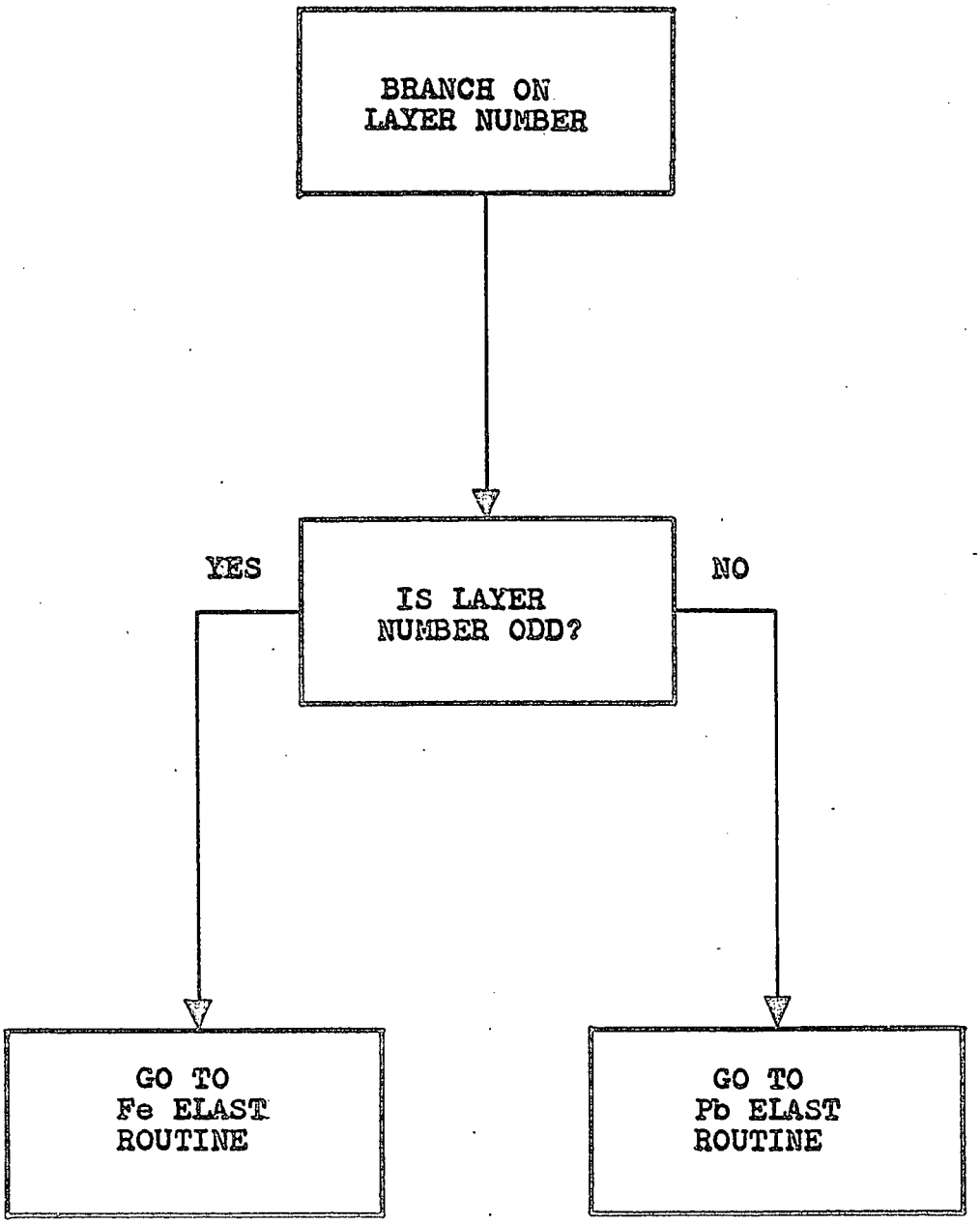
BRANCH ON
LAYER NUMBER
IS LAYER
NUMBER ODD?
YES
NO
GO TO
Fe ELAST
ROUTINE
GO TO
Pb ELAST
ROUTINE

Figure 11. Elast subroutine for Fe

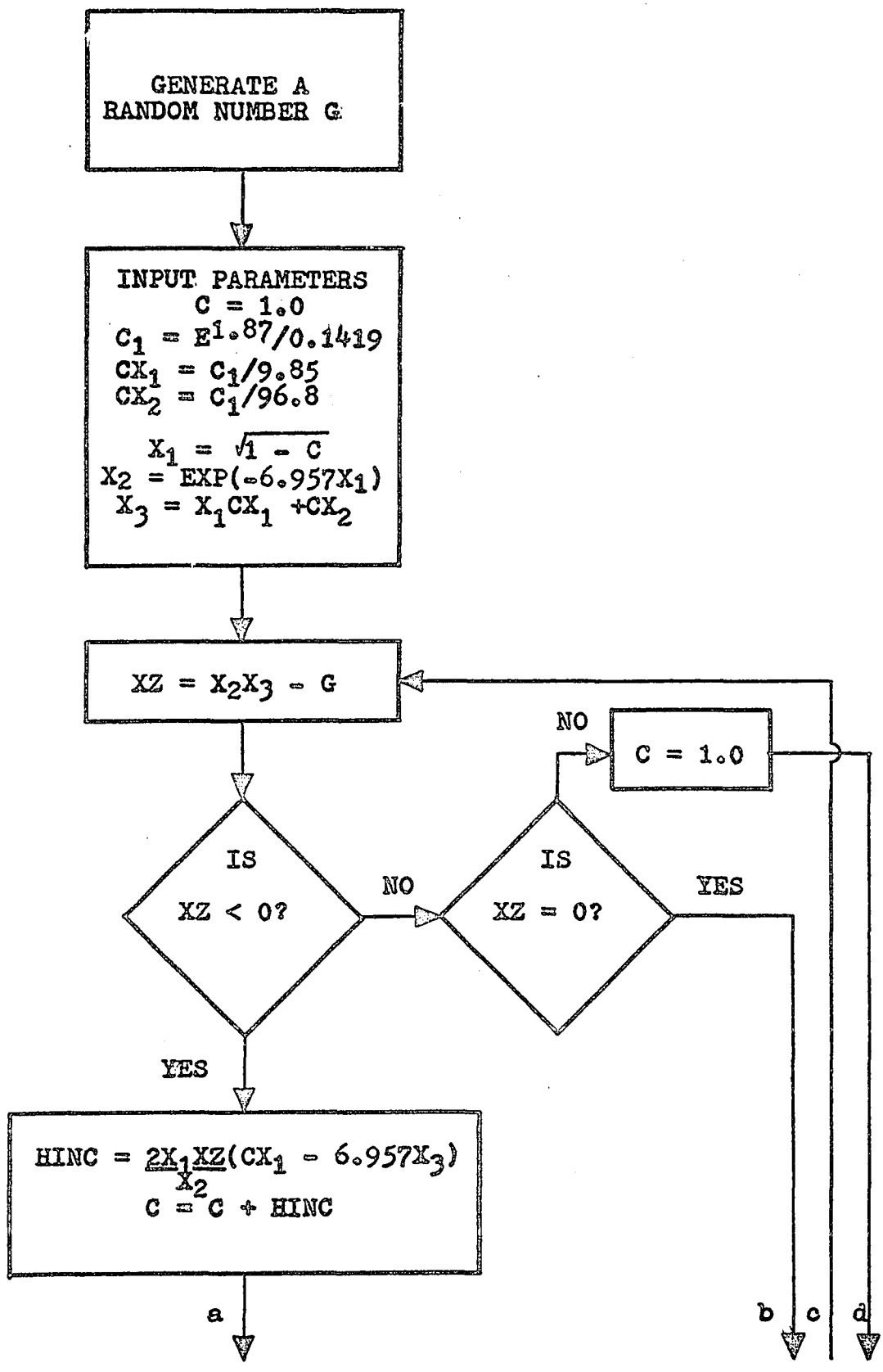
GENERATE A RANDOM NUMBER G
INPUT PARAMETERS
C = 1.0
$C_1 = E^{1.87}/0.1419$
$CX_1 = C_1/9.85$
$CX_2 = C_1/96.8$
$X_1 = \sqrt{1 - C}$
$X_2 = EXP(-6.957X_1)$
$X_3 = X_1CX_1 + CX_2$
XZ = X_2X_3 - G
IS XZ < 0?
NO
IS XZ = 0?
NO
C = 1.0
YES
YES
HINC = $\frac{2X_1XZ(CX_1 - 6.957X_3)}{X_2}$
C = C + HINC
a
b
c
d

Figure 12. Calculation of the elastic scattering angle for Fe

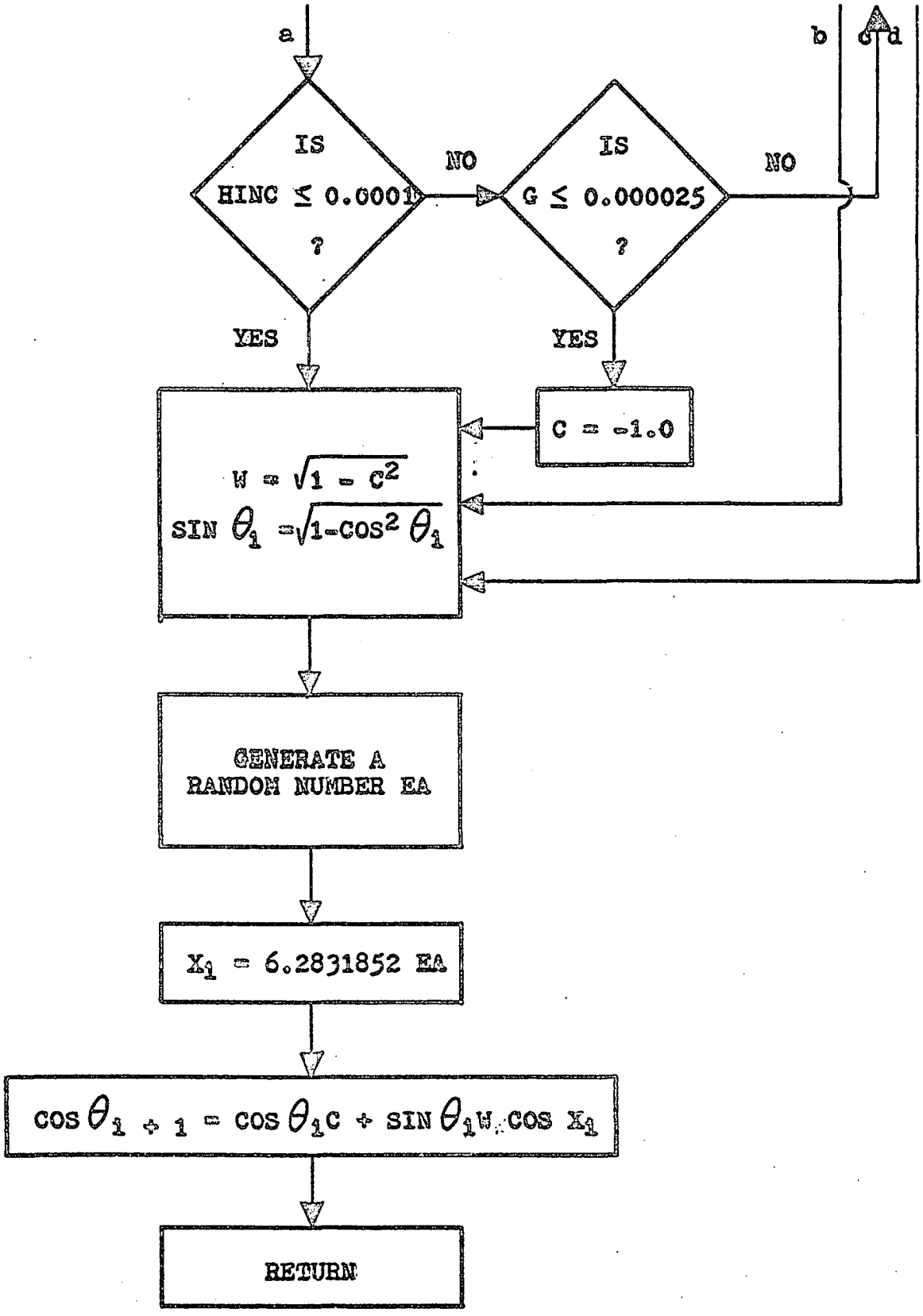
a
b
c
d
IS HINC ≤ 0.0001 ?
NO
IS G ≤ 0.000025 ?
NO
YES
YES
C = -1.0
W = √1 - C²
SIN θ1 = √1-COS² θ1
GENERATE A RANDOM NUMBER EA
X1 = 6.2831852 EA
COS θ1 + 1 = COS θ1C + SIN θ1W. COS X1
RETURN

Figure 13. Elast subroutine for Pb

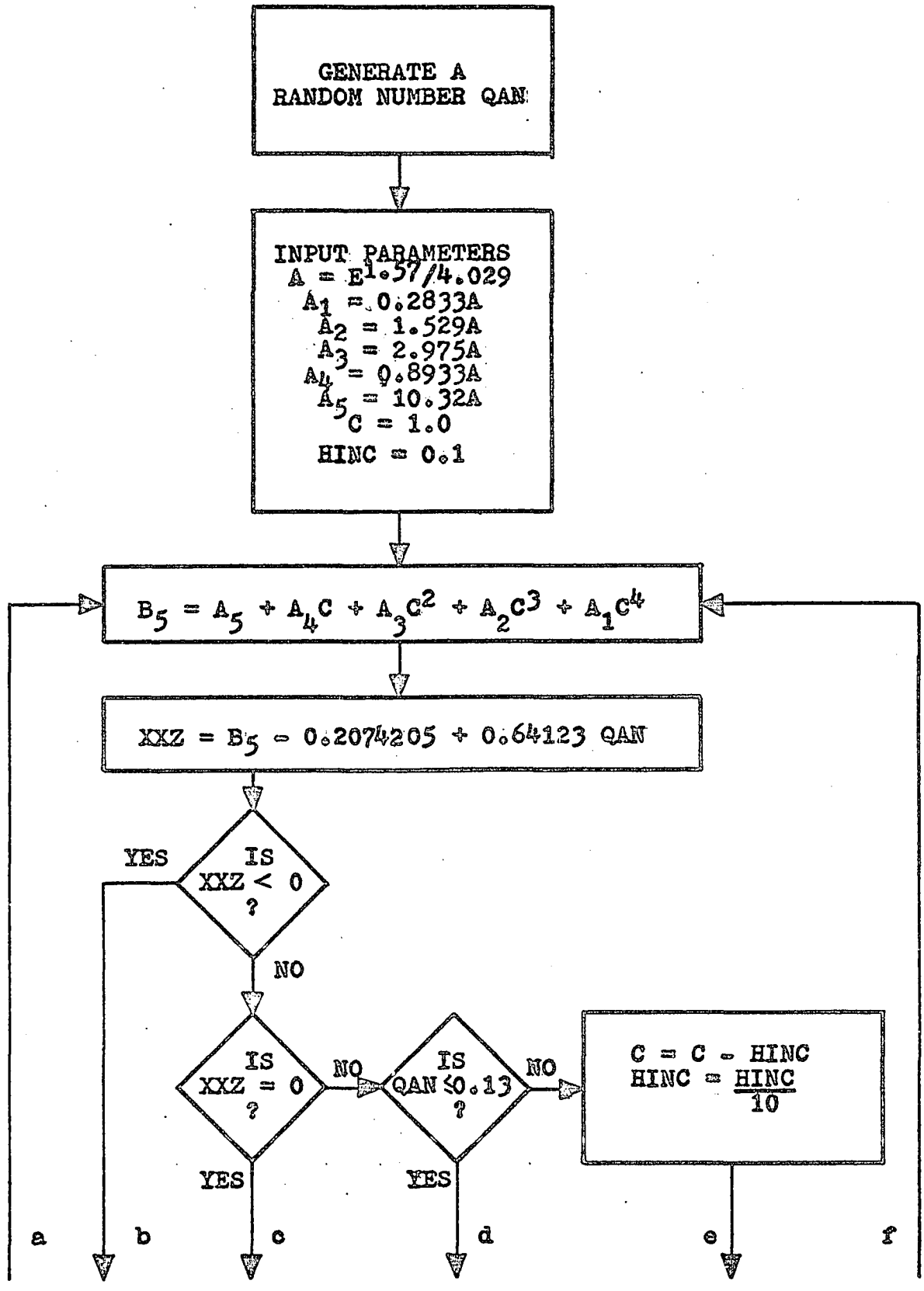
GENERATE A RANDOM NUMBER QAN
INPUT PARAMETERS
A = E^1.57/4.029
A1 = 0.2833A
A2 = 1.529A
A3 = 2.975A
A4 = 0.8933A
A5 = 10.32A
C = 1.0
HINC = 0.1
B5 = A5 + A4C + A3C2 + A2C3 + A1C4
XXZ = B5 - 0.2074205 + 0.64123 QAN
IS XXZ < 0 ?
YES
NO
IS XXZ = 0 ?
NO
IS QAN ≤ 0.13 ?
NO
YES
YES
C = C - HINC
HINC = HINC / 10
a
b
c
d
e
f

Figure 14. Calculation of the elastic scattering angle for Pb

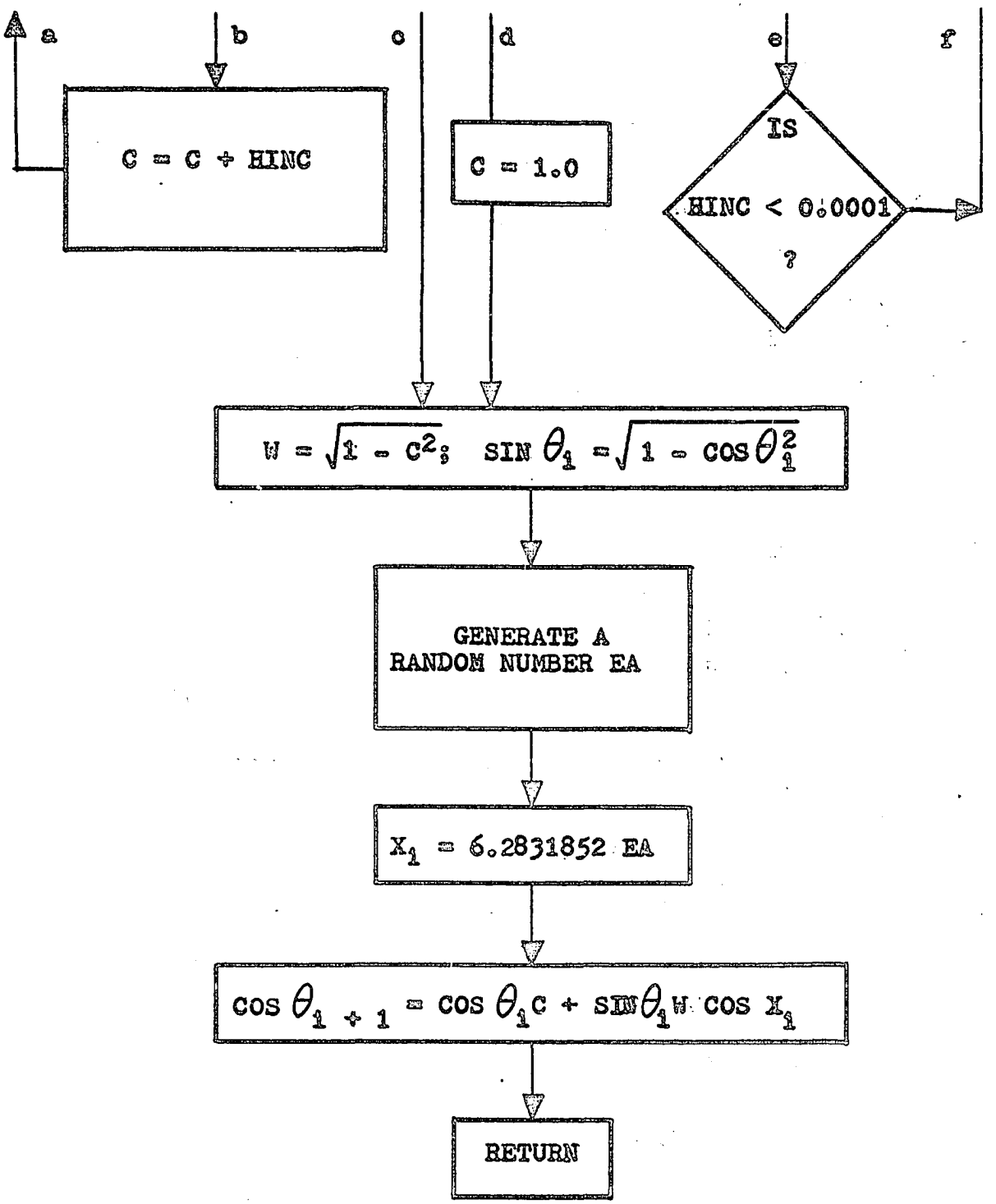
a
b
c
d
e
f
C = C + HINC
C = 1.0
IS
HINC < 0.0001
?
$W = \sqrt{1 - C^2}$; SIN $\theta_1 = \sqrt{1 - \cos\theta_1^2}$
GENERATE A RANDOM NUMBER EA
X_1 = 6.2831852 EA
$\cos\theta_{1+1} = \cos\theta_1 C + \sin\theta_1 W \cos X_1$
RETURN

Figure 15. Energy absorption routine

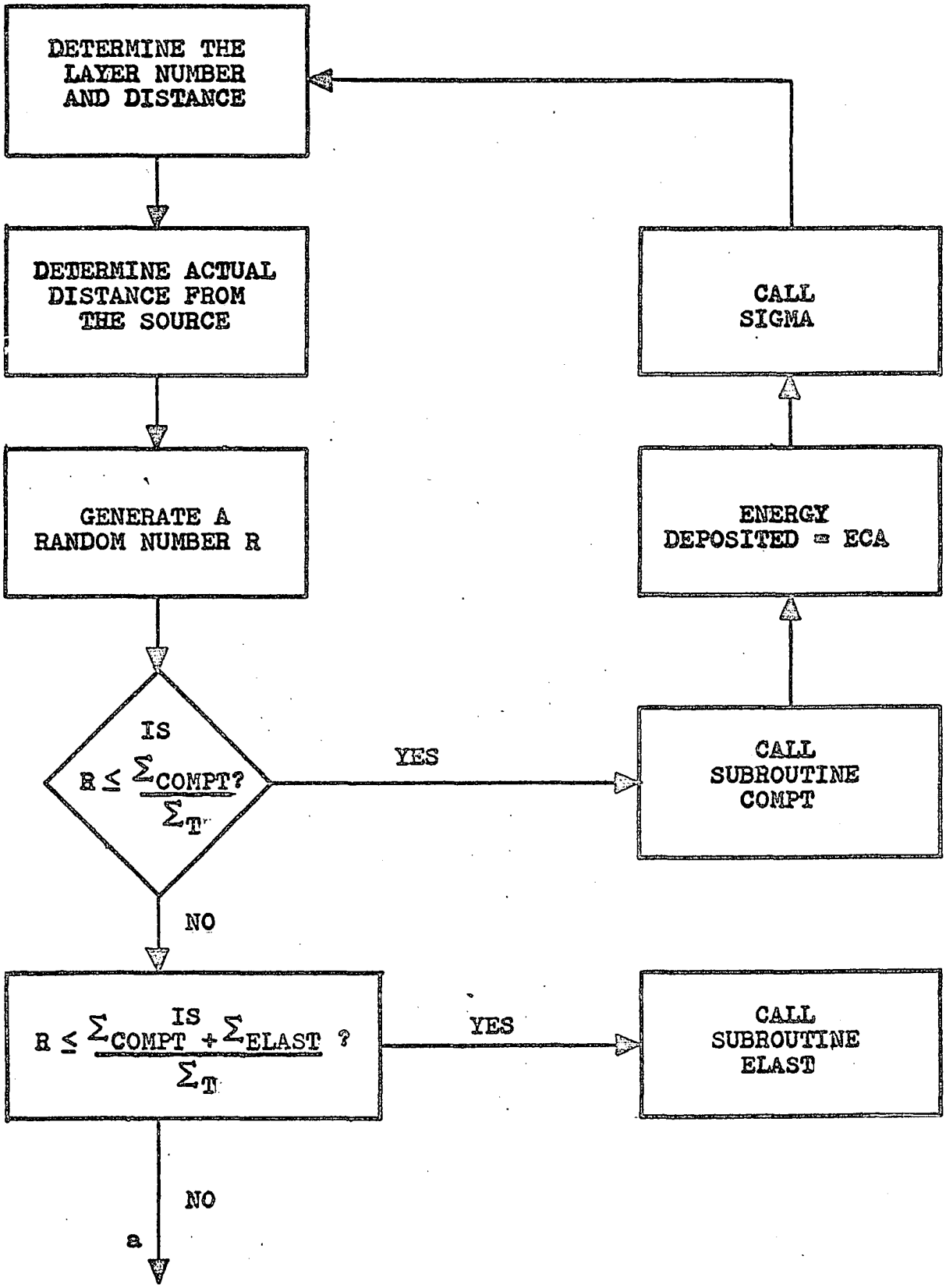
DETERMINE THE LAYER NUMBER AND DISTANCE
DETERMINE ACTUAL DISTANCE FROM THE SOURCE
GENERATE A RANDOM NUMBER R
IS $R \leq \frac{\Sigma_{COMPT}}{\Sigma_T}$?
YES
CALL SUBROUTINE COMPT
NO
IS $R \leq \frac{\Sigma_{COMPT} + \Sigma_{ELAST}}{\Sigma_T}$?
YES
CALL SUBROUTINE ELAST
NO
a
CALL SIGMA
ENERGY DEPOSITED = ECA

Figure 16. Continuation of energy absorption routine to determine total energy absorbed and distance

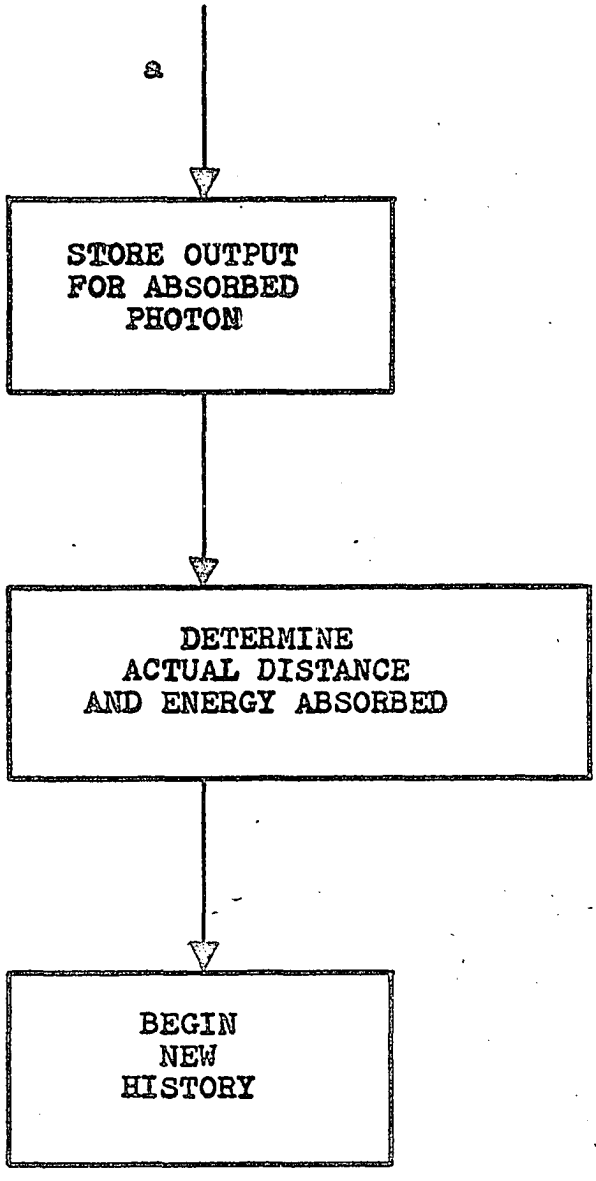
a
STORE OUTPUT FOR ABSORBED PHOTON
DETERMINE ACTUAL DISTANCE AND ENERGY ABSORBED
BEGIN NEW HISTORY

Figure 17. Energy absorption rate as a function of distance from the source (γ = 0.5)

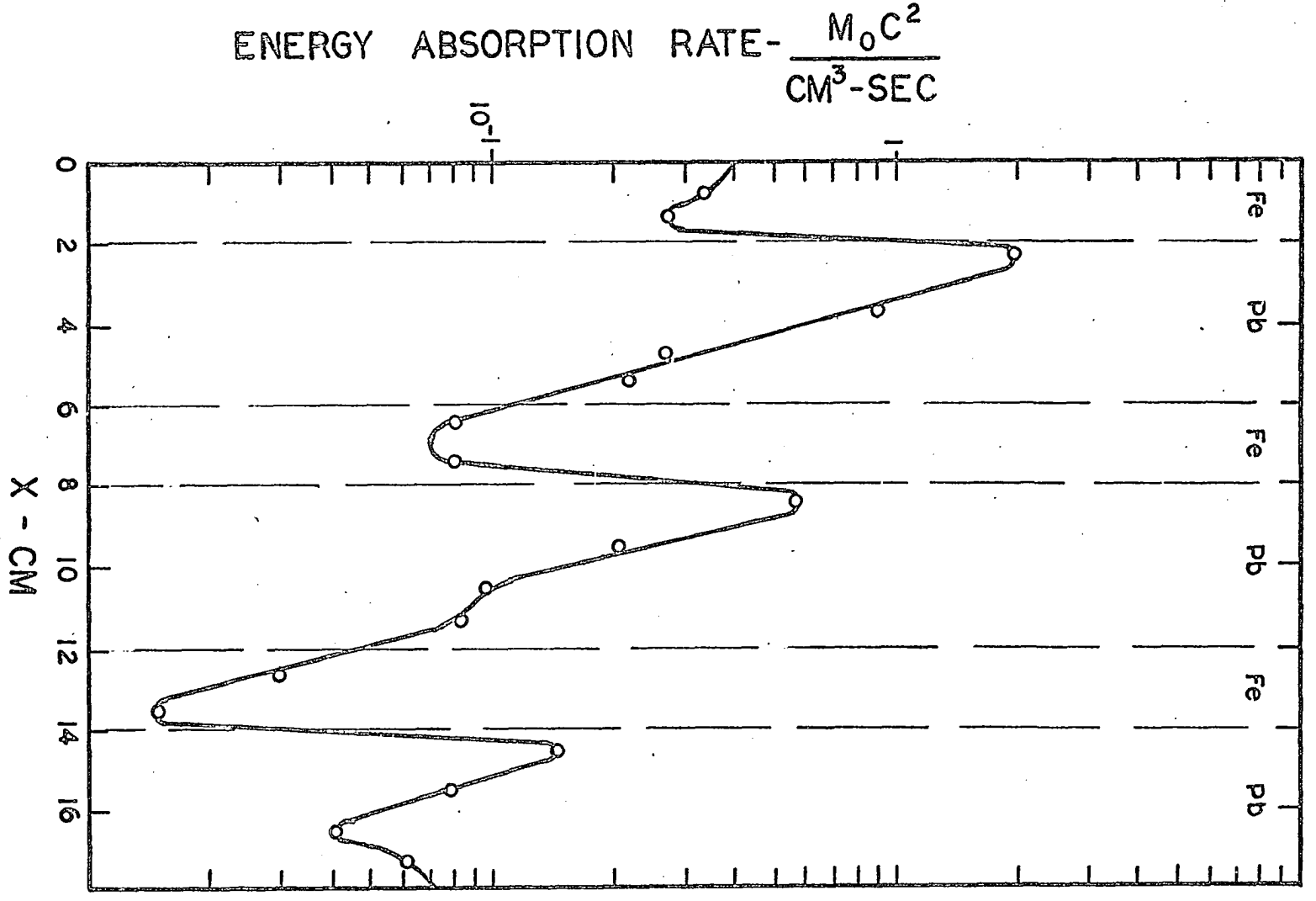
ENERGY ABSORPTION RATE- $\frac{M_0C^2}{CM^3\text{-SEC}}$
10^{-1}
1
X - CM
0
2
4
6
8
10
12
14
16
Fe
Pb
Fe
Pb
Fe
Pb

Figure 18. Energy absorption rate as a function of distance (ν = 1.0)

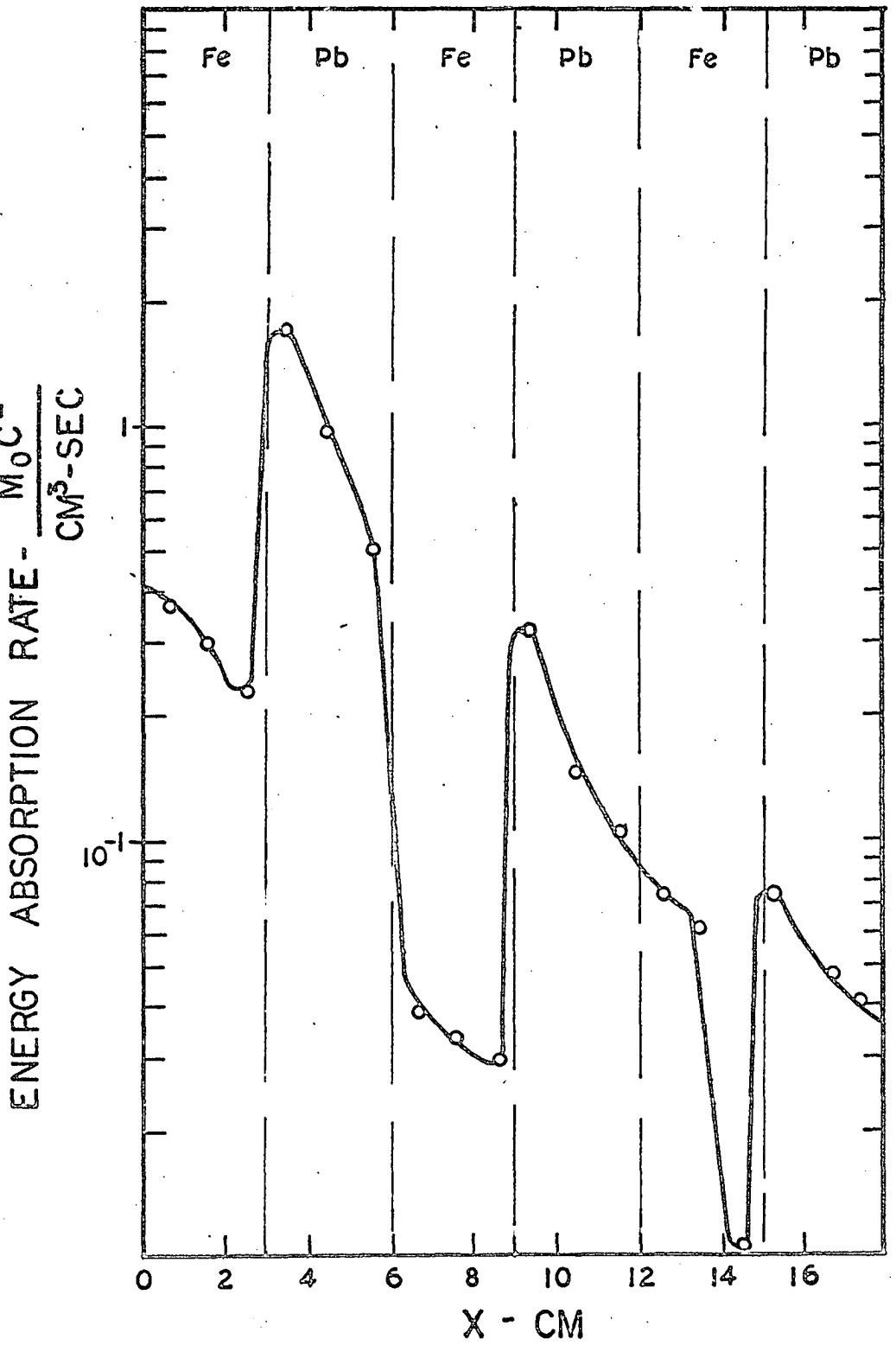
Fe
Pb
Fe
Pb
Fe
Pb
ENERGY ABSORPTION RATE - $\frac{M_0C^2}{CM^3\text{-SEC}}$
1
10^{-1}
0
2
4
6
8
10
12
14
16
X - CM

Figure 19. Energy absorption rate as a function of distance from the source (γ = 2.0)

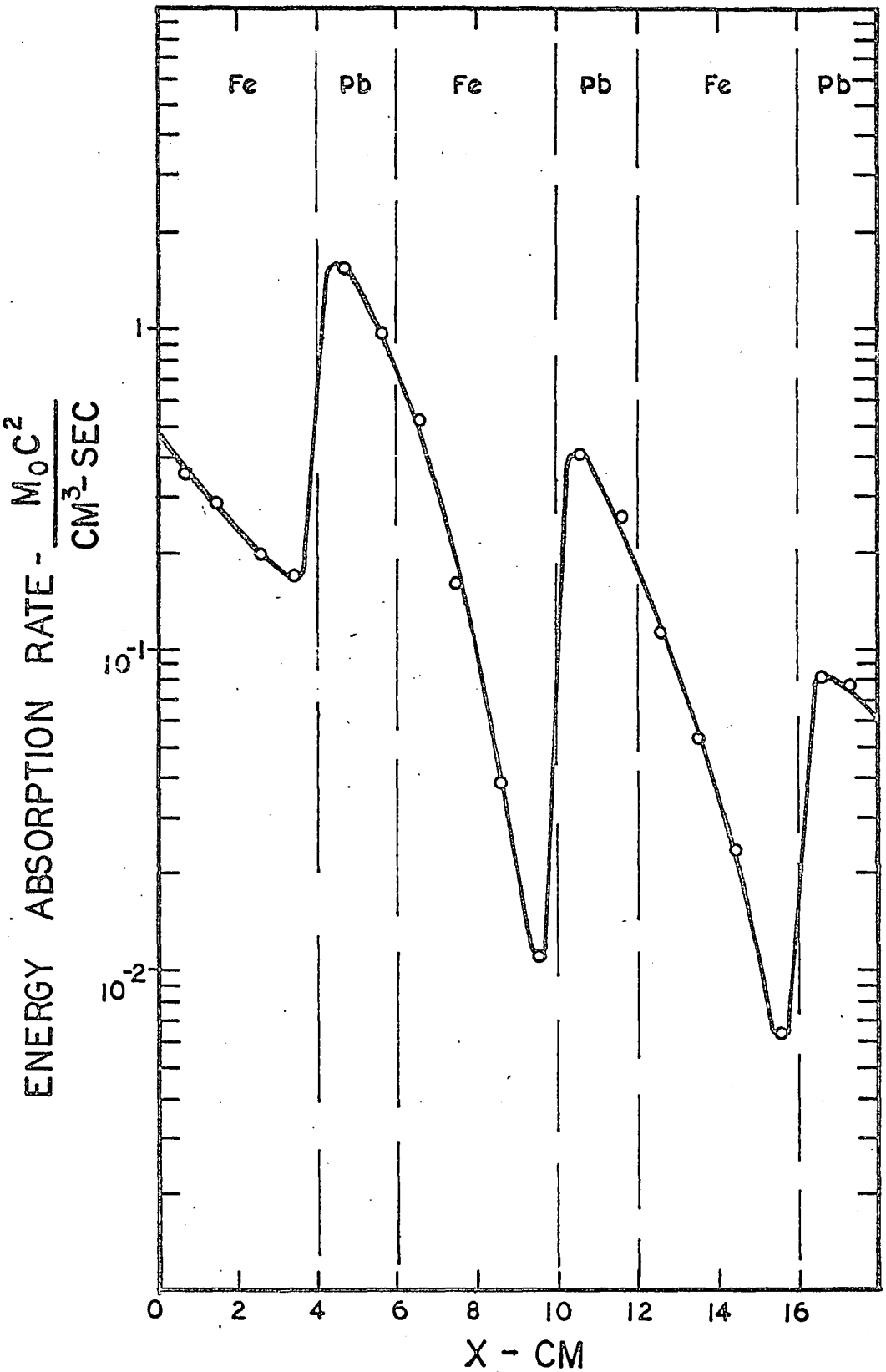
Fe
Pb
Fe
Pb
Fe
Pb
1
10^{-1}
10^{-2}
ENERGY ABSORPTION RATE - $\frac{M_0C^2}{CM^3\text{-}SEC}$
0
2
4
6
8
10
12
14
16
X - CM

Figure 20. Energy absorption rate as a function of distance from the source (γ = 5.0)

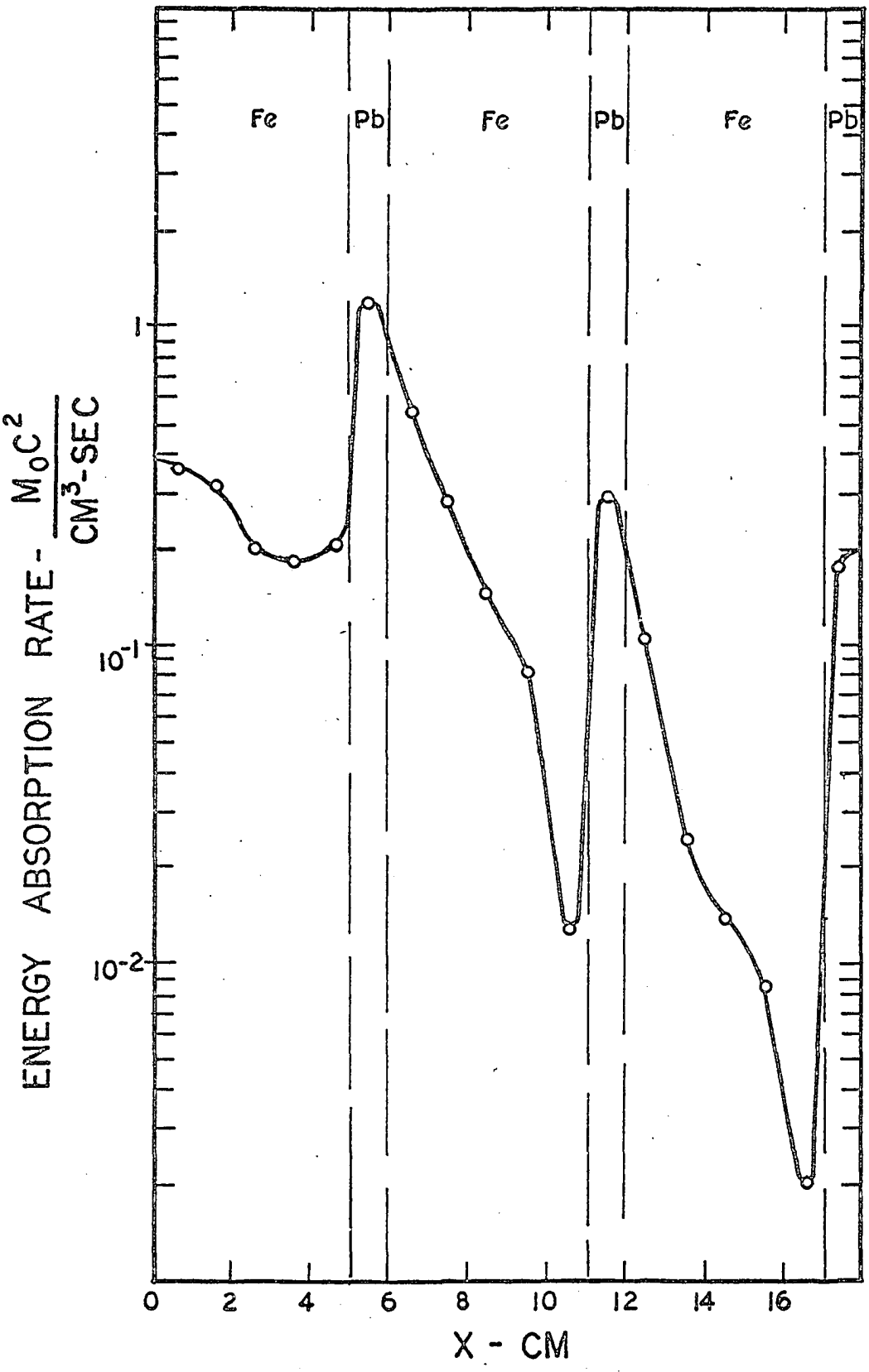
Fe
Pb
Fe
Pb
Fe
Pb
1
10^{-1}
10^{-2}
ENERGY ABSORPTION RATE - $\frac{M_0C^2}{CM^3\text{-}SEC}$
0
2
4
6
8
10
12
14
16
X - CM

Figure 21. Probability of transmission as a function of energy

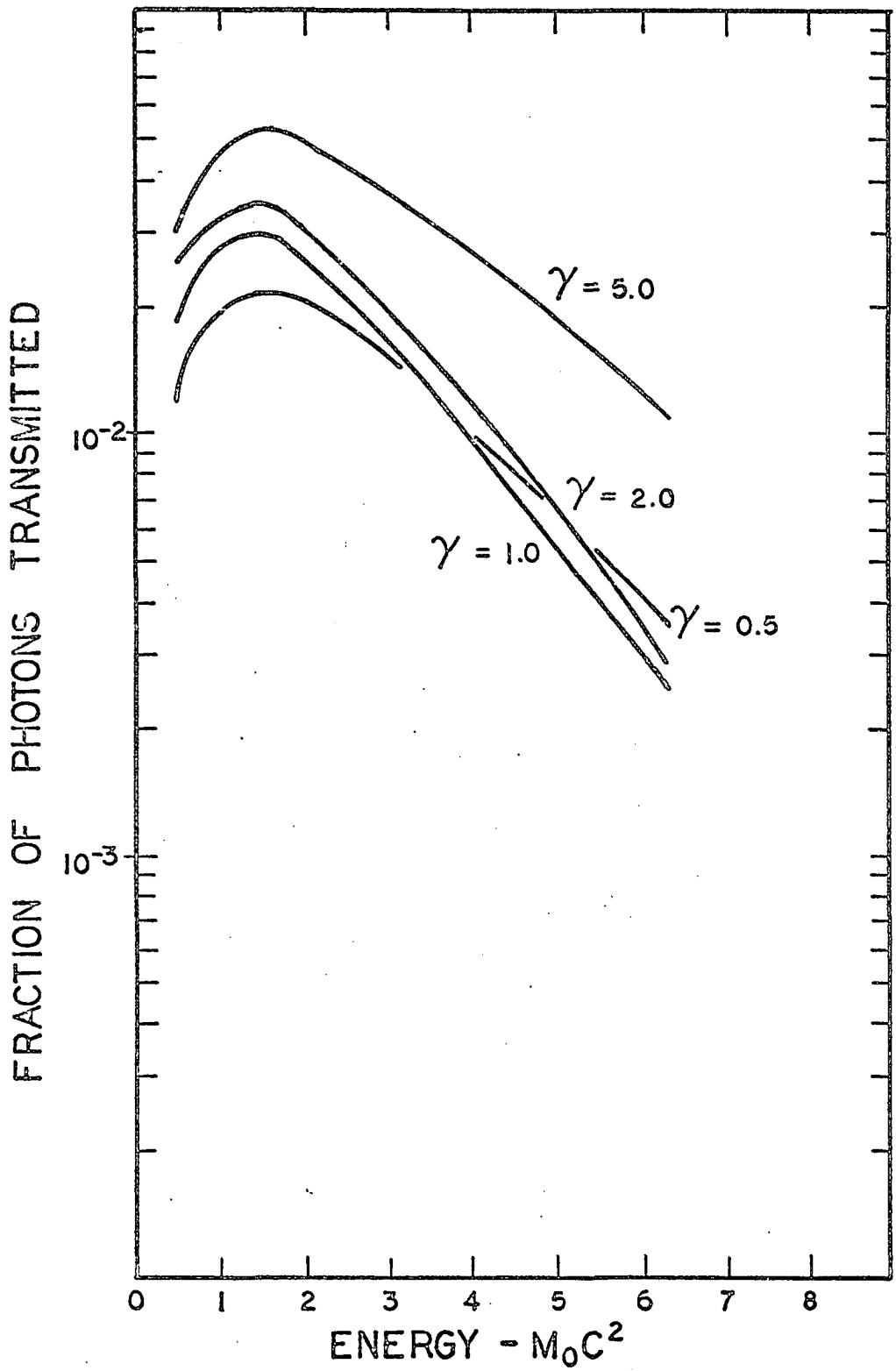
FRACTION OF PHOTONS TRANSMITTED
10^{-2}
10^{-3}
$\gamma = 5.0$
$\gamma = 2.0$
$\gamma = 1.0$
$\gamma = 0.5$
0
1
2
3
4
5
6
7
8
ENERGY - M_0C^2

DISCUSSION OF RESULTS

Data Obtained

The curves for the data obtained from the computer are shown in Figures 17, 18, 19, and 20. These curves represent the energy absorption rate as a function of the distance from the source. The curves are obtained for four different ratios of the thickness of iron slab to the thickness of the adjacent lead slab. They are arranged in increasing order of magnitude for the ratio γ. The data are tabulated in Appendix B.

In all the curves it can be seen that the first peak appears in the first lead slab and the second one appears in the second lead slab. The height of the peak seems to be a function of the ratio γ. As the ratio γ is increased the height of the peak gradually decreases. The height of the peak in the second lead slab is much smaller than that in the first lead slab in all the four runs. In Figures 17, 18, and 19 the third peak in the third lead slab is clearly visible. On the other hand in Figure 20 the third peak is not so clear. This happens because of the large ratio γ. The thickness of the iron slab completely overshadows the thickness of the lead slab.

The data on the fraction of photons transmitted through the entire thickness of the composite shield are given in Table 2 in Appendix B and are plotted in Figure 21.

The most striking feature of this plot is that maxima for all four ratios of thickness occur at an energy of 1.5 moc^2. The maximum increases with the increase in the value of the ratio γ.

The total energy absorbed in each of the four configurations of the composite shields is shown in Table 3 in Appendix B.

For γ = 5.0 the total energy absorbed is smaller than the corresponding values for the remaining three ratios. This is also seen from Figures 20 and 21. In Figure 20 the peak in the first lead slab is shorter than the corresponding peaks in Figures 17, 18, and 19. Therefore, the total energy absorbed in the case of γ = 5.0 is smaller than in the other three cases. Also it is observed in Figure 21 that the maximum for γ = 5.0 is larger than the corresponding maxima for the remaining three γ's.

The interesting feature is the variation in the total energy absorbed as the ratio γ is varied between 0.5 and 2.0. For the values of the ratio γ 0.5, 1.0, and 2.0 the total energy absorbed shows a minimum for γ = 1.0. As γ is varied in either direction about this value, the total energy absorbed increases. This shows that by changing the ratio γ from unity it is possible to absorb more energy in the shield.

For all the four ratios of thickness buildup factors were calculated for the composite shield. These were used along with the average absorption cross section to determine the close rate at the outer edge of the shield. These values are compared with the values obtained from the Monte Carlo calculations. They are shown in Table 4 in Appendix B.

Analysis of Data

There are three different modes by which the history of a photon is terminated. These are (i) absorption in one of the layers of the shield, (ii) transmission across the shield, (iii) reflection of photon into the source region. Mode (i) is determined directly. Modes (ii) and (iii) are determined from the distance at which the photon experiences a collision. If the distance is greater than the total thickness of the shield, it is considered to have followed mode (ii). On the other hand if the distance is less than zero, it is thought of as a consequence of mode (iii).

In order to determine the average number of Compton scatterings per photon before its history is terminated by one of the three modes, a number of test runs were made. The size of each test run was restricted to two hundred photon histories. It was found out that on an average the number of Compton scatterings per photon history were about ten. In some cases this number was as high as eighteen or twenty. But

this happened in very few histories. The energy lost in the scatterings prior to absorption was smaller in comparison with the energy lost in the scatterings in the beginning of the history. A test run usually required between five and six minutes.

The part of the program which needed most of the time was Compt Subroutine. In this subroutine the energy of the photon after it experiences a Compton type collision and the angle of scattering with respect to the x-axis are computed. The expression used in Compt Subroutine is derived earlier and equation 9 gives the relation between E and E' through a random number RAN. This equation is solved by the method of successive iterations. The most striking characteristic of the subroutine is that no approximations to the expression in equation 9 are used. This makes the solution more reliable and the accuracy is considerably improved with respect to previous approximate solutions.

In the test runs along with the number of Compton scatterings, the number of elastic scatterings of photons by the materials of the shield was also studied. This number was small in comparison with the number of Compton scatterings per photon history. Some of the histories in which the number of Compton scatterings was greater than ten, one or two elastic scatterings were observed. In no history did this number exceed two. When the number of Compton scatterings was large

most of the photons were either absorbed in the last two or three centimeters of the shield or they were transmitted. Thus elastic scatterings were responsible in a way for the slight increase in the energy absorption rate near the outer boundary of the shield.

In the test runs which were performed in order to determine the angle of scattering when the photon experiences an elastic scattering collision it was found that the angle was small. In all the test runs it ranged between zero and ten degrees. In a few exceptional cases the angle was about fifteen degrees in iron. It is in agreement with the experimental results of Mann (25).

CONCLUSIONS AND RECOMMENDATIONS

In the problem under investigation use was made of the versatile nature of the Monte Carlo method. In the shield with two infinite dimensions and one finite dimension it was necessary to use only one space coordinate. By specifying the first angle of scattering it was possible to use each photon to generate a history with at least one collision.

Conclusions

1. The problem of the energy absorption rate at various points along the thickness of a laminated shield of iron and lead slabs due to the transmission of gamma radiation from a point isotropic source was successfully attacked by applying the techniques of the Monte Carlo method.
2. The energy absorption rate is dependent upon the ratio of the thickness of the iron slab to that of the adjacent lead slab.
3. For large value of the ratio γ the energy absorption rate is small.
4. Since the energy absorption rate is a function of γ, the total energy absorbed also depends upon γ.
5. It is possible to use the value of the ratio γ in the vicinity of unity to absorb more energy in the shield depending upon the energy emitted by the source of gamma

radiation.

6. Laminated shields should be useful for mobile reactors.

Recommendations

The present investigation can be extended to determine the energy absorption rate due to a plane source of radiation. Also the gamma ray energy distribution in a reactor can be used to determine the energy absorption rate in a laminated shield.

The shield configuration can be changed and either spherical or cylindrical geometry can be used.

Materials other than iron and lead can be studied. A composite shield of three or more materials might turn out to be more effective in absorbing energy than a shield consisting of only two materials.

The ratio γ can be varied to design an asymptotic shield in which γ decreases as the thickness of the shield increases.

REFERENCES CITED

1. Hirschfelder, J. O., Magee, J. L., and Hull, M. H. Physical Review 73:853. 1948.

2. Herschfelder, J. O., Magee, J. L., and Hull, M. H. Physical Review 73:863. 1948.

3. Bethe, H. A., Fano, U., and Karr, P. R. Physical Review 76:538. 1949.

4. Fano, U. Physical Review 76:739. 1949.

5. Peebles, G. H. and Plesset, M. S. Physical Review 81: 430. 1951.

6. Solon, L. R. and Wilkins, J. E., Jr. U. S. Atomic Energy Commission Report NYO-635 New York Operations Office, AEC . 1950.

7. Solon, L. R., Wilkins, J. E., Jr., Oppenheim, A., and Goldstein, H. U. S. Atomic Energy Commission Report NYO-637 New York Operations Office, AEC . 1951.

8. Fano, U., Spencer, L. V., and Berger, M. J. Encyclopedia of Physics 38, Part 2:660. 1959.

9. Goldstein, H. Fundamental aspects of reactor shielding. Reading, Mass., Addison-Wesley Publishing Co., Inc. 1958.

10. Kahn, H. Nucleonics 6, No. 5:27. 1950.

11. Kahn, H. Nucleonics 6, No. 6:50. 1950.

12. Kahn, H. U. S. Atomic Energy Commission Report P-88 Rand Corp., Santa Monica, Calif. . 1949.

13. Meyer, H. A., ed. Symposium on Monte Carlo methods. New York, N.Y., John Wiley and Sons, Inc. 1956.

14. Zerby, C. D. U. S. Atomic Energy Commission Report ORNL-2224 Oak Ridge National Lab., Tenn. . 1956.

15. Beach, L. A., Theus, R. B., Plawchan, J. D., and Faust, W. R. U. S. Atomic Energy Commission Report NRL-4412 Naval Research Laboratory, Washington, D.C. . 1954.

16. Kalos, M. H. U. S. Atomic Energy Commission Report NDA-567 Nuclear Development Corporation of America, White Plains, N. Y. 1956.

17. Nelms, A. T. National Bureau of Standards, Circular 542. 1953.

18. Cashwell, E. T. and Everett, C. J. Monte Carlo method for random walk problems. New York, N. Y., Pergamon Press. 1959.

19. Nelms, A. T. and Oppenheim, I. Journal of Research of the National Bureau of Standards 55:53. 1955.

20. Hildebrand, F. B. Introduction to numerical analysis. New York, N. Y., McGraw-Hill Book Company, Inc. 1956.

21. Brenner, Sheila, Brown, G. E., and Woodward, J. B. Proc. Roy. Soc. London, Series A 227:51. 1954.

22. Brown, G. E. and Mayers, D. F. Proc. Roy. Soc. London, Series A 234:387. 1956.

23. Brown, G. E. and Mayers, D. F. Proc. Roy. Soc. London, Series A 242:89. 1956.

24. Grodstein, G. W. National Bureau of Standards, Circular 583. 1959.

25. Mann, A. K. Physical Review 101:4. 1956.

ACKNOWLEDGEMENTS

The author sincerely wishes to acknowledge his deep gratitude to Dr. Glenn Murphy, his major professor and Head of the Department of Nuclear Engineering for continued support, encouragement, and many helpful suggestions.

Thanks are also due to Dr. D. R. Finch and Mr. Howard Jespersen for their invaluable assistance in the writing of programs for the IBM-7074 digital computer for this investigation.

APPENDIX A

The probability that a photon will travel a distance r without undergoing collision in a material with total cross section $\Sigma_T(E)$ and then collide within a distance dr is given by

$$p(r)dr = e^{-\Sigma_T(E)r}\ \Sigma_T(E)dr \tag{15}$$

If the distance is measured along a direction x with which the direction r makes an angle θ, the probability distribution with x as the variable becomes

$$p(x)dx = \frac{\Sigma_T(E)}{\cos\theta}\ e^{-\frac{\Sigma_T(E)}{\cos\theta}}\ dx \tag{16}$$

Suppose a photon of energy E_i traveling at an angle θ_i with respect to x-axis undergoes an i^{th} collision at x_i. If Δx_{i+1} is the distance between the i^{th} and (i+1)st collision, then:

$$p(\Delta x_{i+1}) = \frac{\Sigma_T(E_i)}{\cos\theta_i}\ e^{-\frac{\Sigma_T(E_i)\ \Delta x_{i+1}}{\cos\theta_i}} \tag{17}$$

$p(\Delta x_{i+1})$ is determined by choosing a random number P which is uniformly distributed between 0 and 1. 1-P is just as good a random number as P observes Goldstein (8). Thus,

$$\left.\begin{aligned} \Delta x_{i+1} &= -\frac{\cos\theta_i\ \ell n\ P}{\Sigma_T(E_i)} \\ x_{i+1} &= x_i + \Delta x_{i+1} \end{aligned}\right\} \tag{18}$$

The general expression for the total macroscopic cross section has the following form:

$$\Sigma_{total} = \Sigma_{compt} + \Sigma_{elast} + \Sigma_{abs} \qquad (19)$$

where

Σ_{total} = total macroscopic cross section

Σ_{compt} = macroscopic Compton cross section

Σ_{elast} = macroscopic elastic scattering cross section

Σ_{abs} = macroscopic absorption cross section.

In order to determine the type of interaction, a random number R is chosen.

If $R < \frac{\Sigma_{compt}}{\Sigma_{total}}$, the interaction is considered to be Compton scattering.

If $\frac{\Sigma_{compt}}{\Sigma_{total}} < R < \frac{\Sigma_{compt} + \Sigma_{elast}}{\Sigma_{total}}$, the interaction is considered to be elastic scattering.

If $R > \frac{\Sigma_{compt} + \Sigma_{elast}}{\Sigma_{total}}$, the interaction is considered to be absorption and the history is terminated.

APPENDIX B

Table 1. Energy absorption rate $\frac{m_o c^2}{cm^3\text{-sec}}$

Distance from source (cm)	γ			
	0.5	1.0	2.0	5.0
0.5	0.3657	0.3958	0.4079	0.3455
1.5	0.2936	0.3158	0.2740	0.3313
2.5	1.8916	0.2245	0.2101	0.1965
3.5	1.04059	1.7464	0.1717	0.1864
4.5	0.3505	1.0149	1.6568	0.2130
5.5	0.2062	0.6214	1.0152	1.1796
6.5	0.07681	0.04504	0.4028	0.5443
7.5	0.08049	0.04064	0.1862	0.2659
8.5	0.5478	0.02924	0.0334	0.1505
9.5	0.2240	0.3397	0.01134	0.07995
10.5	0.1037	0.1819	0.4101	0.01469
11.5	0.08393	0.1315	0.2263	0.3025
12.5	0.03255	0.01834	0.05982	0.08366
13.5	0.01476	0.01659	0.08546	0.02663
14.5	0.1477	0.009047	0.01665	0.01439
15.5	0.07642	0.07589	0.005843	0.007683
16.5	0.04182	0.05155	0.08419	0.002037
17.5	0.06707	0.04114	0.07765	0.1883

Table 2. Energy distribution of transmitted photons

Energy ($m_o c^2$)	0.5	1.0	2.0	5.0
	Fraction of photons transmitted			
0.5	1.2272×10^{-2}	1.978×10^{-2}	2.6363×10^{-2}	3.1362×10^{-2}
1.5	2.2272×10^{-2}	3.145×10^{-2}	3.5454×10^{-2}	5.3182×10^{-2}
2.5	1.2272×10^{-2}	1.656×10^{-2}	2.4545×10^{-2}	3.5454×10^{-2}
3.5	7.227×10^{-3}	1.01×10^{-2}	1.591×10^{-2}	2.727×10^{-2}
4.5	7.727×10^{-3}	6.06×10^{-3}	9.091×10^{-3}	2.727×10^{-2}
5.5	3.636×10^{-3}	2.02×10^{-3}	3.636×10^{-3}	1.5×10^{-2}
6.5	4.545×10^{-3}	2.01×10^{-3}	2.727×10^{-3}	1.181×10^{-2}
7.5	1.363×10^{-3}	1.212×10^{-3}	1.01×10^{-3}	7.575×10^{-3}
8.5	1.727×10^{-3}			3.181×10^{-3}

Table 3. Total energy absorbed $\frac{m_o c^2}{cm^2\text{-sec}}$

	$\frac{m_o c^2}{cm^2\text{-sec}}$	$\frac{gm}{cm^2}$	$\frac{m_o c^2}{sec \cdot gm}$
0.5	5.6453	183.0	0.03082
1.0	5.2997	177.6	0.02985
2.0	5.3210	162.2	0.03275
5.0	4.1331	146.9	0.02810

Table 4. Dose rate at the outer edge of the shield

	Buildup factor	Dose rate calculated	$\frac{m_o c^2}{cm^3\text{-sec}}$ this work
0.5	3.0	0.210	0.06707
1.0	2.0	0.116	0.04114
2.0	2.3	0.117	0.07765
5.0	2.2	0.094	0.1883